ADVANCING EARTH AND SPACE SCIENCES

JGR Solid Earth

RESEARCH ARTICLE

10.1029/2024JB030817

Impact-Driven Redox Stratification of Earth's Mantle

Estefania L. Henningsen[1], **Jun Korenaga**[1], **and Simone Marchi**[2]

[1]Department of Earth and Planetary Sciences, Yale University, New Haven, CT, USA, [2]Department of Space Studies, Southwest Research Institute, Boulder, CO, USA

Key Points:

- We evaluate two proposed mechanisms (metal layer and droplets) for magma ocean oxidation and calculate $Fe^{3+}/\Sigma Fe$ during Earth formation
- We find that the metal layer mechanism is too short lived to oxidize the mantle, whereas droplets may leave the mantle much too oxidized
- To achieve present-day bounds on mantle oxidation state, the Moon-forming impact is not likely to have melted the whole mantle

Supporting Information:

Supporting Information may be found in the online version of this article.

Correspondence to:

E. L. Henningsen,
estefania.larsen@yale.edu

Citation:

Henningsen, E. L., Korenaga, J., & Marchi, S. (2025). Impact-driven redox stratification of Earth's mantle. *Journal of Geophysical Research: Solid Earth*, *130*, e2024JB030817. https://doi.org/10.1029/2024JB030817

Received 21 NOV 2024
Accepted 18 MAR 2025

Author Contributions:

Conceptualization: Jun Korenaga
Formal analysis: Estefania L. Henningsen
Funding acquisition: Jun Korenaga, Simone Marchi
Investigation: Estefania L. Henningsen
Methodology: Estefania L. Henningsen
Software: Estefania L. Henningsen
Supervision: Jun Korenaga
Visualization: Estefania L. Henningsen
Writing – original draft: Estefania L. Henningsen
Writing – review & editing: Estefania L. Henningsen, Jun Korenaga, Simone Marchi

Abstract Planetary formation involves highly energetic collisions, the consequences of which set the stage for the ensuing planetary evolution. During accretion, Earth's mantle was largely molten, a so-called magma ocean, and its oxidation state was determined by equilibration with metal-rich cores of infalling planetesimals through redox buffering reactions. We test two proposed mechanisms (metal layer and metal droplets) for equilibration in a magma ocean and the resulting oxidation state ($Fe^{3+}/\Sigma Fe$). Using scaling laws on convective mixing, we find that the metal layer could promote oxidation of a magma ocean, but this layer is too short-lived to reproduce present-day mantle $Fe^{3+}/\Sigma Fe$ (2%–6%). Metal droplets produced by the fragmentation of impactor cores can also promote oxidation of a magma ocean. We use Monte Carlo sampling on two possible accretion scenarios to determine the likely range of oxidation states by metal droplets. We find that equilibration between silicate and metal droplets tends toward higher mantle $Fe^{3+}/\Sigma Fe$ than presently observed. To achieve present-day mantle $Fe^{3+}/\Sigma Fe$ and maintain the degree of equilibration suggested by Hf-W and U-Pb systematics (30%–70%), the last (Moon-forming) giant impact likely did not melt the entire mantle, therefore leaving the mantle stratified in terms of oxidation state after main accretion completes. Furthermore, late accretion impacts during the Hadean (4.5–4.0 Ga) could generate reduced domains in the shallow upper mantle, potentially sustaining surface environments conducive for prebiotic chemistry.

Plain Language Summary Earth's bulk composition was largely set during Earth's formation. Highly energetic impacts by planetesimals during planetary formation would melt the proto-Earth mantle and produce magma oceans. Metal from impactor cores and the proto-Earth magma ocean chemically interact and give rise to the mantle's oxidation state. We test two hypotheses (metal layer and metal droplets) for metal-silicate chemical equilibration within a magma ocean to determine the resulting oxidation state of the mantle. Our results show that the metal layer hypothesis requires time scales longer than the lifetime of the layer to promote oxidation of Earth's mantle given present-day constraints. In comparison, the metal droplets hypothesis could promote oxidation of Earth's mantle, but likely necessitated incomplete mantle melting or low efficiency of equilibration. In particular, the last giant impact may only have melted part of the mantle, and therefore left a chemically stratified mantle in terms of oxidation state.

1. Introduction

The oxidation state of Earth's mantle (as measured by $Fe^{3+}/\Sigma Fe$) was likely established during planetary formation by chemical equilibration with accreted metal (Frost et al., 2008; Hirschmann, 2012). The final stage of primary accretion involved large-scale collisions that are expected to have produced magma oceans (Abe, 1993), allowing for rapid metal-silicate equilibration (Rubie et al., 2003). After accretion, the resulting oxidation state would modulate the Hadean surface environment and the atmosphere (Gaillard et al., 2022; Hirschmann, 2012; Schaefer et al., 2024; Sossi et al., 2020). Metal-silicate equilibration in a magma ocean is hypothesized to occur in the mid-mantle, owing to the equilibration pressure derived from the mantle abundance of moderately siderophile elements (e.g., Fischer et al. (2015)). It has been proposed that metal-silicate equilibration in a magma ocean occurs through two possible mechanisms: a metal-layer overlying a solidified mantle or metal droplets falling through a magma ocean (Rubie et al., 2003) (Figure 1). Although early building blocks for Earth were likely highly reduced ($Fe^{3+}/\Sigma Fe \sim 0.004$) (Rubie et al., 2011), studies have shown that metal-silicate equilibration through a metal-layer (Figure 1c), if it occurred in a single-stage, would likely lead to an oxidized magma ocean ($Fe^{3+}/\Sigma Fe > 0.02$) (Armstrong et al., 2019; Deng et al., 2020). The efficacy of this mechanism depends critically on the longevity of the metal layer, which may be severely limited by Rayleigh-Taylor instabilities (Rubie et al., 2003).

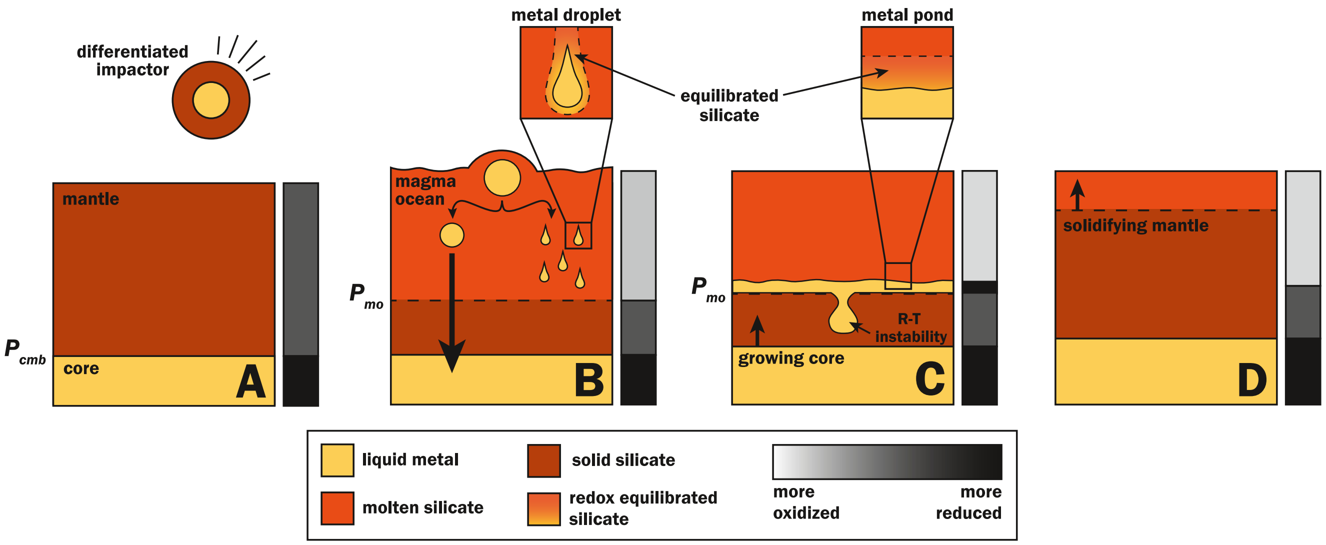

Figure 1. A model depiction of the oxidation of the mantle during accretion by metal-silicate equilibration in a magma ocean. The gray-scale bars next to each panel show relative oxidation state for each layer in the proto-Earth. Color key shown at the bottom of the figure. (a) A differentiated impactor collides with the proto-Earth, where P_{cmb} designates the proto-Earth core-mantle boundary. The mantle is initially relatively reduced (dark gray). (b) The impact melts part of the mantle, where P_{mo} designates the base of the magma ocean. The impactor silicate material is added to the proto-Earth's mantle and the impactor core fragments through Rayleigh-Taylor instability in the magma ocean. A portion of the impactor core may be poorly fragmented and quickly sequestered to the proto-Earth core (demonstrated by thick black arrow). Efficiently fragmented parts of the core form metal droplets that descend through the magma ocean and equilibrate with surrounding silicate melt. The magma ocean increases in oxidation state (light gray). (c) Droplets form a short-lived metal layer resting on the solidified mantle. The layer equilibrates with silicate melt above it, further increasing the oxidation state of the magma ocean. The time scale for the metal layer is short so the oxidation state of the magma ocean does not change significantly during this stage (minor change in light gray shade for oxidation state). Metal diapirs form by Rayleigh-Taylor instability and merge with the proto-Earth core. The proto-Earth core grows through the addition of impactor core metal (through immediate sequestration shown in panel b and from diapirs in panel c). (d) The magma ocean solidifies. As convection is sluggish in solid mantle, the mantle remains redox stratified for some time after cooling.

Equilibration by the descent of accreted metal through the magma ocean (metal droplets scenario, Figure 1b) depends on the stochastic outcome of accretionary collisions. The details of accretion, however, are still debated (Halliday & Canup, 2023). The final phase of primary accretion is thought to be characterized by multiple giant impacts, with the last being the Moon-forming event. The late accretion stage followed (Morbidelli & Wood, 2015), adding a total mass of up to ~2% Earth mass (Marchi et al., 2018). Large planetesimals (greater than a few 100 km in diameter) would have been differentiated, with a silicate mantle and an iron core (Neumann et al., 2018). Upon impact, planetesimal cores may get fragmented down to centimeter- to millimeter-sized droplets in the magma ocean (Deguen et al., 2014; Landeau et al., 2021; Stevenson, 1990). Metal droplets sink rapidly (~0.5 m s^{-1}) and approach chemical equilibrium with surrounding silicate melt (Deguen et al., 2014; Rubie et al., 2003). Whereas a single droplet equilibrates only a small amount of melt, the total amount of metal from planetesimal cores could equilibrate with much of the magma ocean. In the metal droplets scenario, the mid-mantle equilibration pressure can be regarded as an effective pressure around which droplets equilibrate with melt (Hirschmann, 2012; Rubie et al., 2003).

In this study, we examine the oxidation state of the magma ocean through metal-silicate equilibration during accretion. Whereas previous studies have presumed a metal layer as the mechanism for magma ocean oxidation, we show that the layer's short lifetime limits its oxidation potential. Metal droplets could efficiently equilibrate with the magma ocean, but studies with a metal droplets model (e.g., Rubie et al., 2003) have not examined oxidation state in reference to $Fe^{3+}/\Sigma Fe$. We demonstrate that metal droplets could produce a wide range of oxidation states for the mantle, with two major consequences. First, the stochastic nature of impacts during primary accretion (including the Moon-forming giant impact) makes it possible to create stratification in terms of oxidation state in the mantle. Such stratification appears to be required to explain both the present-day abundances of moderately siderophile elements and the oxidation state of the mantle. A possible consequence of redox stratification is that a more reduced upper mantle would result in the long-term release of reducing volcanic gases, suppressing oxygen accumulation in the early atmosphere. Second, large late accretion impacts may have produced localized regions of even more reduced shallow mantle, leading to a transient reducing surface environment. This regional reducing environment has important consequences for prebiotic evolution in the Hadean.

2. Equilibrium $Fe^{3+}/\Sigma Fe$ in a Magma Ocean

In a magma ocean, core-forming metal and silicate equilibrate through the following reaction:

$$\mathrm{Fe_{metal}} + \frac{1}{2}\mathrm{O_2} \leftrightarrow \mathrm{FeO_{silicate}} \tag{1}$$

By Equation 1, the concentrations of metal Fe and silicate FeO set the magma ocean oxygen fugacity (f_{O_2}) at equilibrium. For example, 8 wt. % FeO results in an oxygen fugacity of about two log units below the iron-wüstite buffer ($\Delta IW = -2$, where ΔIW represents the difference between f_{O_2} and the IW buffer in log units) (Hirschmann, 2021). Oxygen fugacity controls the relative abundance of Fe^{2+} (as FeO) and Fe^{3+} (as $FeO_{1.5}$) in silicate melt by the following reaction:

$$\mathrm{FeO_{silicate}} + \frac{1}{4}\mathrm{O}_2 \leftrightarrow \mathrm{FeO_{1.5,silicate}} \tag{2}$$

This series of redox buffering reactions are sometimes referred to as the disproportionation of $FeO_{silicate}$ into Fe_{metal} and $FeO_{1.5,silicate}$. Given pressure, temperature, and composition, we determine the molar fractions of FeO and $FeO_{1.5}$ in silicate using the following parameterization (Hirschmann, 2022):

$$a \ln f_{O_2} = \log_{10}\frac{X^{melt}_{FeO_{1.5}}}{X^{melt}_{FeO}} - b - \frac{c}{T} + \frac{\Delta C_p}{R\ln(10)}\left[1 - \frac{T_0}{T} - \ln\left(\frac{T}{T_0}\right)\right] + \frac{\int_{P_0}^{P}\Delta V dP}{RT\ln(10)} - \frac{1}{T}\left[Y_1X_{SiO_2} + Y_2X_{TiO_2} + Y_3X_{MgO} + Y_4X_{CaO} + Y_5X_{NaO_{0.5}} + Y_6X_{KO_{0.5}} + Y_7X_{PO_{2.5}} + Y_8X_{SiO_2}X_{AlO_{1.5}} + Y_9X_{SiO_2}X_{MgO}\right]. \tag{3}$$

Here a, b, c, ΔC_p, R, T_0, and Y_n are constants (Table S1 in Supporting Information S1). Variables in Equation 3 that we control or calculate are oxygen fugacity (f_{O_2}), molar fractions for $FeO_{1.5}$ and FeO ($X^{melt}_{FeO_{1.5}}$ and X^{melt}_{FeO}), temperature (T), difference in molar volume (ΔV), pressure (P), and composition (X_{oxide}). These are described in more detail below.

For P and T, we apply a parameterization of magma ocean adiabats with pyrolytic composition (Korenaga, 2023; Miyazaki & Korenaga, 2019b) (Figure 2a). This parameterization best models existing experimental data on silicate melts at high P and T conditions (Miyazaki and Korenaga (2019a) and references therein). Our parameterization implies magma ocean freezing from the bottom-up but, depending on the exact freezing mechanisms, a basal magma ocean with enriched FeO content may be possible (Boukaré et al., 2018; Miyazaki & Korenaga, 2019a). For model simplicity, we do not incorporate a basal magma ocean. The existence of an FeO-enriched basal magma ocean would stabilize Fe^{3+} at high pressures and temperatures (Figure 2b). As such, our choice in adiabats without a basal magma ocean leads to a conservative estimate for mantle Fe^{3+}. For the metal layer scenario, we test both 3,500 and 4,500 K mantle potential temperature. For the metal droplets scenario, we chose a potential temperature of 3,500 K based on modeling of impact-generated magma oceans (Korenaga & Marchi, 2023). For this scenario, we also tested a second method where the magma ocean is assumed to be at a potential temperature that crosses liquidus at its base (Figures S1–S3 and S4c–S4d in Supporting Information S1). The main text reports results with the first method; similar results are obtained with the second one.

For the difference in molar volumes ΔV between FeO and $FeO_{1.5}$, we use thermodynamic modeling of P-V-T conditions for $(Mg,Fe)SiO_3$ melt from Deng et al. (2020) (their Figure 1). For the integration involving $\Delta V(P,T)$ in Equation 3, we determine ΔV by interpolation for all pressures at a constant temperature for each point on the adiabat.

For oxygen fugacity, f_{O_2}, we adopt the parameterization for the IW buffer from Hirschmann (2021). This parameterization extrapolates smoothly to higher temperatures but is only calibrated to 100 GPa. Beyond

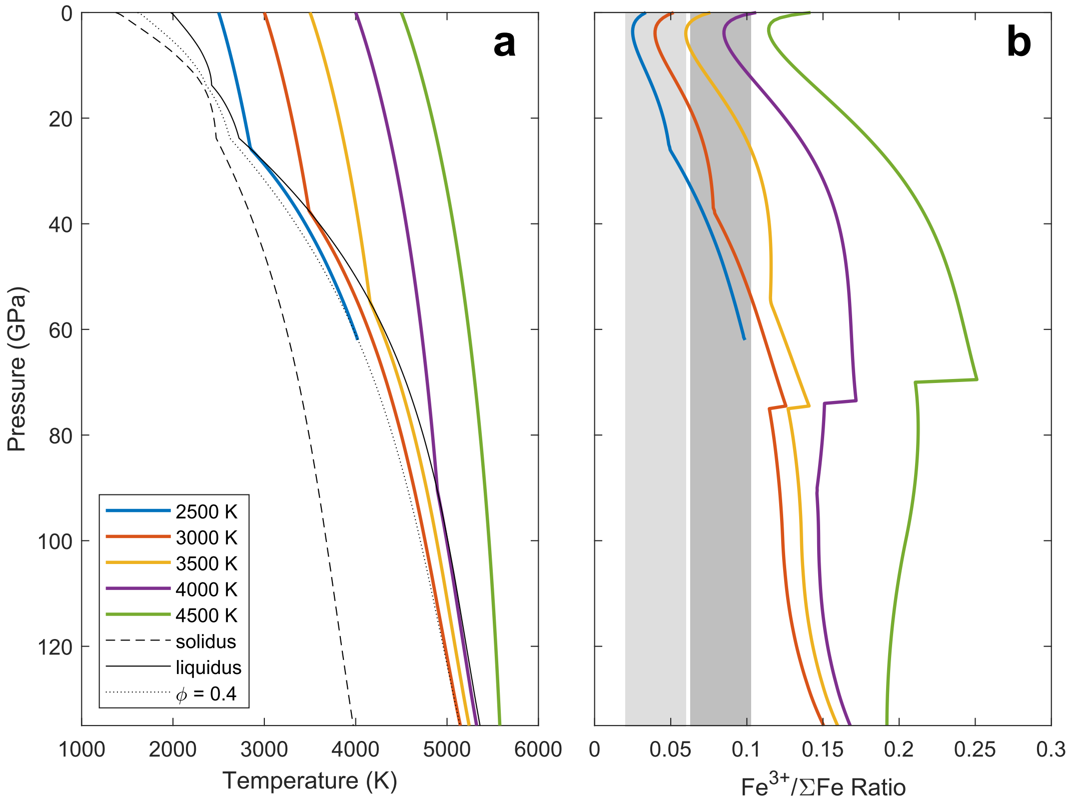

Figure 2. Geotherms and $Fe^{3+}/\Sigma Fe$ ratio as a function of pressure and temperature. (a) Geotherms for a range of mantle potential temperatures (2,500–4,500 K), with solidus (dashed), liquidus (black solid), and 40% melt fraction (dotted), based on the experimental and theoretical studies of mantle melting (Korenaga, 2023; Miyazaki & Korenaga, 2019a, 2019b). For most of our analysis, the 3,500 K geotherm is used as it remains above the melt fraction through depth and within the scope of potential temperatures for impact-generated magma oceans (Korenaga & Marchi, 2023). (b) Corresponding $Fe^{3+}/\Sigma Fe$ for $\Delta IW = -2$ as a function of pressure and temperature given by geotherms in (a) and final Earth composition from Rubie et al. (2011). Light gray shading indicates present-day estimates on the $Fe^{3+}/\Sigma Fe$ ratio for the whole mantle (2%–6%) (Frost & McCammon, 2008; Hirschmann, 2022). Dark gray shading is the respective region for present-day estimates but before chromium oxidation (Hirschmann, 2022). This effect from Cr oxidation is incorporated into our metal droplets modeling. The discontinuity seen near 70 GPa is due to the change in Gibbs energy during phase transition between *fcc/bcc* iron to *hcp* iron in our choice of IW buffer parameterization (Hirschmann, 2021). The 2,500 K geotherm truncates at a pressure of approximately 60 GPa due to surpassing the critical melt fraction of 40%, below which our analysis of oxygen fugacity become uncertain.

100 GPa, we chose to linearly extrapolate the IW buffer as it best matches the trend given by Campbell et al. (2009) compared to its analytical counterpart (Figure S6 in Supporting Information S1). For our metal layer modeling, we set oxygen fugacity at $\Delta IW = -2$ at the base of the magma ocean. In our metal droplets modeling, we estimate ΔIW during accretion by:

$$\Delta IW = 2\log\left(\frac{X_{FeO}^{MW}}{X_{Fe}^{metal}}\right), \tag{4}$$

where X_{FeO}^{MW} is the mole fraction of FeO in magnesiowüstite and X_{Fe}^{metal} is the mole fraction of Fe in core-destined metal. We determine X_{FeO}^{MW} using parameterization of mole fraction of FeO in silicate ($X_{FeO}^{silcate}$) from Rubie et al. (2011).

In Equation 3, X_{oxide} represents mole fractions of components in silicate melt (e.g., $X_{FeO}^{silcate}$). In our metal layer modeling, we use the composition of Deng et al. (2020) for the magma ocean. Using an alternative composition (Armstrong et al., 2019) would not change our metal layer results significantly as the $Fe^{3+}/\Sigma Fe$ versus P or T changes very little (Figure S7 in Supporting Information S1). In our metal droplets modeling, we use the composition for the growing Earth (both core and mantle) by the heterogenous accretion model from Rubie et al. (2011) (their Figure 4 and Supplementary Data Tables S3a and S3b; our Table S4 in Supporting Information S1). For impactor mantle composition, we also apply the model of Rubie et al. (2011) where impactors are distinguished as "early" or "late" (their Supplementary Data Table S3a; our Table S5 in Supporting Information S1). In this scheme, "early" impactors are comparably less oxidized that "late" impactors. The exact composition, volatile budget, and degree of oxidation for impactors remains an open question (e.g., Halliday and Canup (2023); Martins et al. (2023); Newcombe et al. (2023); Steller et al. (2022)). For our modeling, the choice of impactor composition has a minor effect on final mantle oxidation state. Using a homogenous composition for impactors throughout the whole of accretion changes final $Fe^{3+}/\Sigma Fe$ ratio by ±0.005.

Using Equation 3, we calculate the $Fe^{3+}/\Sigma Fe$ ratio for $\Delta IW = -2$ as a function of pressure and temperature using the final Earth composition from Rubie et al. (2011) (Figure 2b). We choose an oxygen fugacity of $\Delta IW = -2$ because this represents the likely oxygen fugacity during the final stage of core-formation (Frost et al., 2008). The stabilization of Fe^{3+} under magma ocean conditions has been observed experimentally (Armstrong et al., 2019; H. L. Zhang, Hirschmann, et al., 2024; Zhang et al., 2017) and through first-principles calculations (Deng et al., 2020). The exact behavior or FeO and $FeO_{1.5}$ at high pressures and temperatures is an active area of research and warrants future work (Hirschmann, 2022). Recent experimental work (H. L. Zhang, Hirschmann, et al., 2024) was able to place tighter constraints on the pressure dependence of $Fe^{3+}/\Sigma Fe$ in silicate melts up to 70 GPa, and made minor updates to the equation of state we employ here (Deng et al., 2020). The equation of state (EOS) of H. L. Zhang, Hirschmann, et al. (2024) predicts higher $Fe^{3+}/\Sigma Fe$ than that of Deng et al. (2020) beyond 40 GPa. Additionally, the behavior of $Fe^{3+}/\Sigma Fe$ at higher temperatures is still poorly constrained experimentally (H. L. Zhang, Hirschmann, et al., 2024). We chose to use the EOS of Deng et al. (2020) as a conservative estimate for $Fe^{3+}/\Sigma Fe$ at deep magma ocean conditions. Our aim is to determine the possible range of $Fe^{3+}/\Sigma Fe$ during metal-silicate equilibration in a magma ocean through various mechanisms and the general observed trend toward higher $Fe^{3+}/\Sigma Fe$ at higher temperatures and pressures is most important for our work.

3. Magma Ocean Equilibration by a Metal Layer

We first investigate the feasibility of magma ocean oxidation through a metal layer scenario (Figure 1c). To this end, we assess the possibility of obtaining present-day mantle $Fe^{3+}/\Sigma Fe$ through convective mixing of equilibrated silicate at the boundary with unequilibrated magma ocean. Prior studies (Armstrong et al., 2019; Deng et al., 2020) have imposed an oxygen fugacity of $\Delta IW \sim -2$ at a certain equilibration pressure, corresponding to the depth of a metal layer in a magma ocean. Silicate equilibrates with the metal layer and obtains a corresponding $Fe^{3+}/\Sigma Fe$ by redox buffering reactions (1) and (2). Prior studies have assumed that the equilibrated $Fe^{3+}/\Sigma Fe$ is the same throughout the magma ocean, which in turn implicitly assumes that both convective mixing and chemical diffusion are sufficiently fast. We do not make this assumption and calculate the rate at which silicate equilibrates and mixes by convective scaling (Solomatov, 2015) to deduce the time-dependent evolution of $Fe^{3+}/\Sigma Fe$ in the magma ocean.

The equilibration rate (in the unit of kg/s) by one convection cell in a magma ocean, J_n, is:

$$J_n = \frac{V\rho_{Si}}{n\tau_n}, \tag{5}$$

where ρ_{Si} is silicate melt density, τ_n is the time needed to travel horizontally along the bottom boundary of the cell, n is the total number of cells, and V is the volume of the diffusion-limited spherical shell at the bottom with radius R and thickness h. The shell radius, R, is calculated as the core radius, $R_{c,0}$, plus the distance from the CMB to the base of the magma ocean. We estimate the shell thickness by the diffusion length scale, $h \sim \sqrt{D\tau_n}$, where the chemical diffusivity, D, ranges between 10^{-9} and 10^{-7} m^2 s^{-1} (Poe et al., 1997; Posner et al., 2017; Rubie et al., 2003). The value of τ_n can be expressed as $\tau_n = \frac{L}{v}$, where L is the characteristic horizontal distance and v is the convective velocity. We approximate the number of convection cells by assuming the base of a convection cell occupies a square patch with area L^2 on the surface of the diffusion-limited spherical shell. The number of convection cells can be estimated then as $4\pi R^2/L^2$. For a whole-mantle magma ocean ($L = 2{,}900$ km) and $R = R_c$, there would be ~17 convection cells. As this is merely an approximation, we chose to explore $n = 10$, 20, and 40.

For convective velocity, v, we adopt the scaling relation for soft turbulence (Solomatov, 2015):

$$v \approx 0.6\left(\frac{\alpha g L_m \Phi}{\rho_{Si} C_p}\right)^{\frac{1}{3}} \tag{6}$$

where Φ is the convective heat flux, given as

$$\Phi \approx 0.089\left(\frac{k(T_m - T_s)}{L_m}\right) Ra^{\frac{1}{3}}. \tag{7}$$

In above, α is thermal expansivity, g is the gravitational acceleration, L_m is the depth of magma ocean, C_p is specific heat capacity, k is thermal conductivity, T_m is magma ocean potential temperature, T_s is surface temperature, and Ra is the Rayleigh number (Table S2 in Supporting Information S1). Surface temperature T_s will depend on mantle potential temperature and the rate of radiative cooling into space. Based on an early Hadean atmosphere composition, Miyazaki and Korenaga (2022) calculated surface temperature for a magma ocean using a 1-D radiative-convective atmosphere model from Nakajima et al. (1992), which can be parameterized as (Korenaga, 2023):

$$T_s = c_0 + c_1 T_m, \tag{8}$$

where $c_0 = 546$ K and $c_1 = 0.63$. Combining above into Equation 5 results in an equilibration rate per convection cell J_n, and multiplying this with the number of cells yields the *net* mass flow rate (Figure S5 in Supporting Information S1).

To determine the evolution of $\mathrm{Fe}^{3+}/\Sigma\mathrm{Fe}$ in the magma ocean, we calculate the rate of change of $\mathrm{Fe}^{3+}/\Sigma\mathrm{Fe}$ as:

$$\frac{dr}{dt} = \frac{nJ_n}{M_{mo}}(r_{eq} - r), \tag{9}$$

where r is the magma ocean $\mathrm{Fe}^{3+}/\Sigma\mathrm{Fe}$, r_{eq} is the $\mathrm{Fe}^{3+}/\Sigma\mathrm{Fe}$ equilibrium ratio with $\Delta\mathrm{IW} = -2$ at the depth of the CMB or metal layer (Equation 3), and M_{mo} is the mass of the magma ocean. We assume that the magma ocean starts highly reduced ($r(0) = 1 \times 10^{-3}$), mimicking the oxidation state of accreted material. Due to turbulent convection, whole magma ocean overturn occurs on the scale of days (Solomatov, 2015), so the change in bulk magma ocean $\mathrm{Fe}^{3+}/\Sigma\mathrm{Fe}$ from mixing is fast given the time interval of our calculation ($\Delta t = 10$ kyr). The resulting $\mathrm{Fe}^{3+}/\Sigma\mathrm{Fe}$ after mixing at each time step is used to calculate the oxygen fugacity using Equation 3 at the surface of the magma ocean.

A whole-mantle magma ocean in chemical equilibrium with the core-mantle boundary (CMB) could produce a highly oxidized magma ocean with a large $\mathrm{Fe}^{3+}/\Sigma\mathrm{Fe}$ value between 0.15 and 0.20 in a few million years (Figure 3). However, such duration is unlikely because the magma ocean solidifies from the bottom and loses contact with the core within 1 kyr (Miyazaki & Korenaga, 2019b; Solomatov, 2015). Tidal heating has been suggested to lengthen the magma ocean phase (Zahnle et al., 2015), but tidal heating becomes effective only after the magma ocean starts to solidify (Korenaga, 2023), thus unaffecting the above timing constraint. Given less than 1 kyr for core-contact equilibration, this limits oxidation by this mechanism, leaving the magma ocean much too reduced to replicate present-day conditions.

Alternatively, a mid-mantle metal layer may form at the base of the magma ocean, resting above the solidified mantle (i.e., the melt-solid mixture past the rheological transition where melt fraction $\phi < 0.4$ (Solomatov, 2015)). The depth of this layer would correspond to the equilibration depth proposed from metal-silicate equilibration of moderately siderophile elements (Fischer et al., 2015; Li & Agee, 1996; Zhang et al., 2017). This metal layer is denser and gravitationally unstable, therefore prone to form diapirs or dikes to eventually merge with the core (Rubie et al., 2015). If this layer is reasonably long-lived, the overlying silicate melt may chemically equilibrate with the metal. Our convective mixing results show that a mid-mantle layer could also produce an oxidized magma ocean in a few million years (Figure 4). The longevity of the mid-mantle metal layer is critical to whether present-day $\mathrm{Fe}^{3+}/\Sigma\mathrm{Fe}$ can be achieved through this mechanism. We evaluate the longevity of the metal layer by

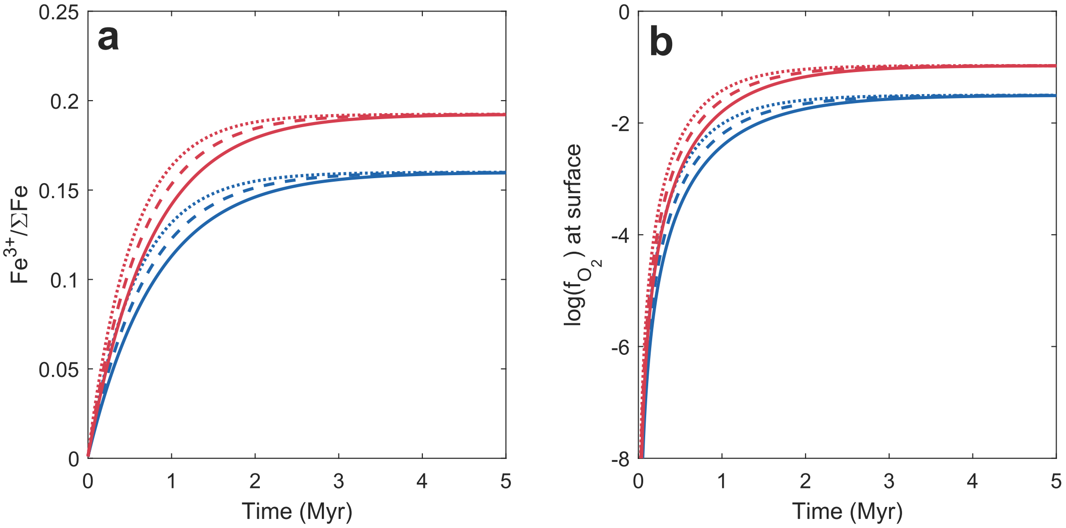

Figure 3. The $Fe^{3+}/\Sigma Fe$ ratio (a) and $\log f_{O_2}$ at the surface (b) over time of a magma ocean with whole-mantle convective mixing and chemical equilibration with the core-mantle boundary. Mantle potential temperatures are 4,500 K (red) and 3,500 K (blue). The number of convection cells used is 10 (solid), 20 (dashed), and 40 (dotted). A value of 10^{-7} m^2 s^{-1} is used for chemical diffusivity in all cases. A magma ocean $Fe^{3+}/\Sigma Fe$ between 0.06 and 0.10 would be required to replicate present-day mantle conditions (see Figure 2b).

assessing its Rayleigh-Taylor instability. We use parameterization for a self-gravitating viscous sphere (Mondal & Korenaga, 2018) where the instability growth rate, σ, is:

$$\sigma = 10^{-10.13} R^{1.86} L_{Fe}^{0.047} \rho_s^{0.87} (\rho_{Fe} - \rho_s)^{1.3} \mu_s^{-0.98} \mu_{Fe}^{-0.054}, \tag{10}$$

where R represents the radius from the center of Earth to the metal layer depth, L_{Fe} is the thickness of the layer, ρ_s is the density of the underlying mantle, ρ_{Fe} is the density of the metal, and μ_s and μ_{Fe} are the viscosities of the underlying mantle and metal, respectively. The density of the solidified mantle (ρ_s) is estimated from the Preliminary Reference Earth Model (PREM) (Dziewonski & Anderson, 1981) and the density of the metal (ρ_{Fe}) is estimated as 7,800 kg/m^3 (Rubie et al., 2003). The viscosity of mantle at the rheological transition, μ_s, is likely somewhere between 10^{13} and 10^{18} Pa s (Miyazaki & Korenaga, 2019b; Solomatov, 2015), so we use an intermediate value of 10^{15} Pa s. For the metal layer, we assume its viscosity, μ_{Fe}, is similar to the outer core, ~0.01 Pa s (de Wijs et al., 1998). For the thickness of the metal layer, L_{Fe}, we use a range of 1 m–100 km (Karato & Murthy, 1997; Rubie et al., 2003; Wood et al., 2006). With $\mu_s = 10^{15}$ Pa s, instability time is on the order of hours (Figure 5). A greater silicate viscosity would reduce the growth rate, and therefore increase the time until instability. Increasing μ_s to 10^{18} Pa s increases instability time to only on the order of hundreds of days. It is difficult to justify a time scale of millions of years necessary for complete chemical equilibration shown in Figure 4, thus leaving behind a more reduced mantle than previously suggested (Armstrong et al., 2019; Deng et al., 2020).

4. Magma Ocean Equilibration by Metal Droplets

Although a metal layer suffers from a short lifetime, accreted metal may still equilibrate with silicate during its descent though the magma ocean. Earth's primary accretion is estimated to have lasted about 50–100 million years, with each impact adding up to a few percent of present-day Earth mass (Halliday, 2004; Nesvorný et al., 2021). The last (Moon-forming) giant impact likely occurred between 30 and 120 Myr and may have added upwards of 50% Earth mass (Canup et al., 2023). Late accretion followed, adding small but appreciable mass (up to ~2% Earth mass) (Marchi et al., 2014, 2018). We test the resulting oxidation state of the mantle through the descent of metal droplets during accretion. As the details of accretion are still debated (Halliday & Canup, 2023), we test two accretion models through Monte Carlo sampling.

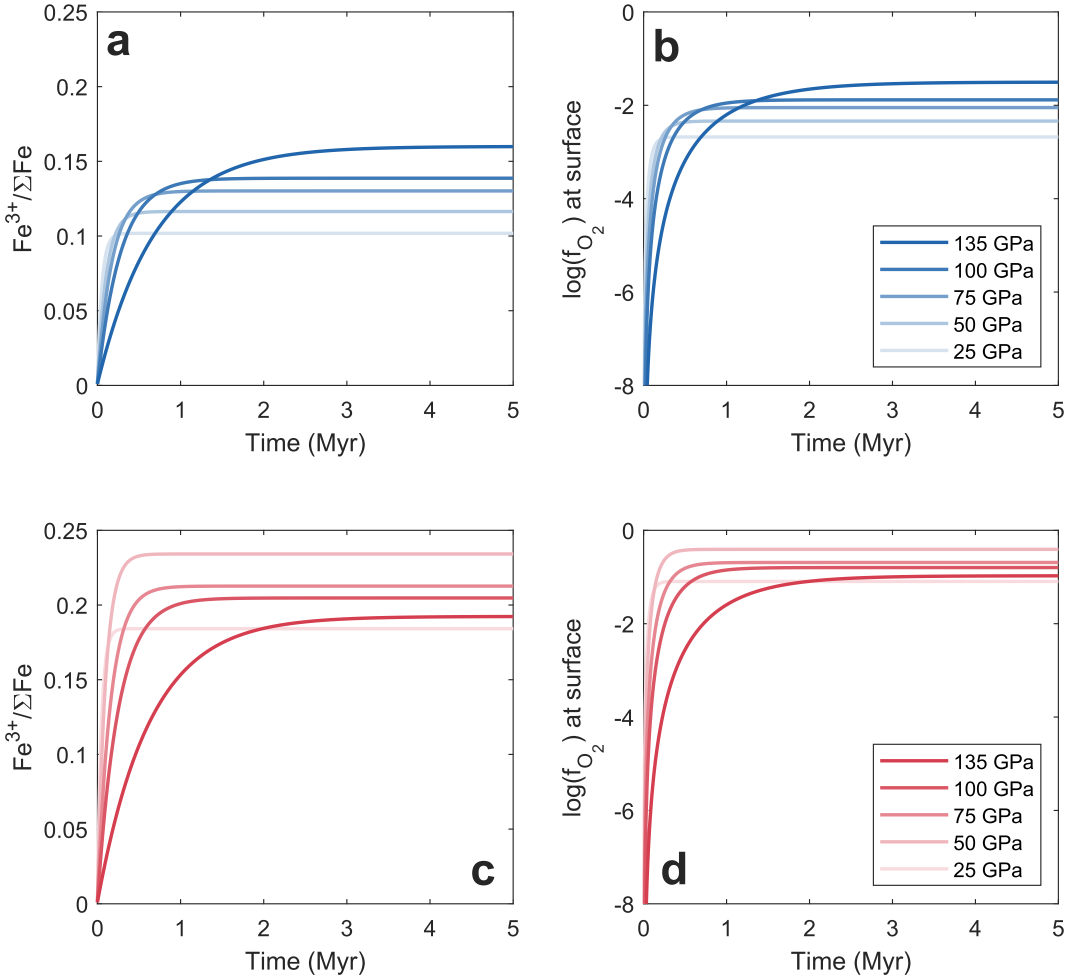

Figure 4. The $Fe^{3+}/\Sigma Fe$ ratio (a and c) and $\log f_{O_2}$ at the surface (b and d) of the magma ocean due to chemical equilibration with a metal layer at varying depths. Figures (a) and (b) use a 3,500 K mantle potential temperature and figures (c) and (d) use 4,500 K. All results use 20 convective cells and 10^{-7} m^2 s^{-1} chemical diffusivity. Note the 25 GPa approaches the 135 GPa results when using the 4,500 K geotherm because the $Fe^{3+}/\Sigma Fe$ equilibrium ratio decreases with depth at this temperature (Figure 2b).

4.1. Accretion Modeling

A variety of Earth accretion models exist (Halliday, 2004; Kleine et al., 2009; Nesvorný et al., 2021; O'Brien et al., 2018; Rudge et al., 2010; Wetherill, 1990; Zube et al., 2019) and estimates for the age of the Moon vary between 30 and 200 Myr (Barboni et al., 2017; Borg et al., 2015; Thiemens et al., 2019). We chose to evaluate two accretion models corresponding to the extremes in the Moon-forming impactor mass but with similar ages for the timing of the impact. The first model, H04 (Halliday, 2004), involves discrete impact events with a moderate growth curve (63% mass by 19 Myr), an age of the Moon at 55 Myr after Solar System formation, and an impactor:proto-Earth mass ratio of 1:10 (Figure 6a, inset). The second model, N21 (Nesvorný et al., 2021), has fast initial growth (50% mass by 5 Myr), an age of the Moon at 41 Myr, and an impactor:proto-Earth mass of 1:1 (Figure 6b, inset). Fast accretion models struggle to explain the tungsten isotope anomaly within Earth's mantle (Nimmo et al., 2010; Zube et al., 2019), but we include model N21 due to the continued prevalence of similar models in planetary formation literature (Canup, 2012; Canup et al., 2023). After the last giant impact, both models reach $0.99M_{E,0}$, to account for a 1% mass addition during late accretion. To model the mass of the growing core during accretion, we use the Earth core mass fractions given in Rubie et al. (2011) (their Supplementary Data Table S3b). Given Earth mass, M_E, from accretion curve and core mass, M_c, from Rubie et al. (2011), we can calculate mantle mass, M_m:

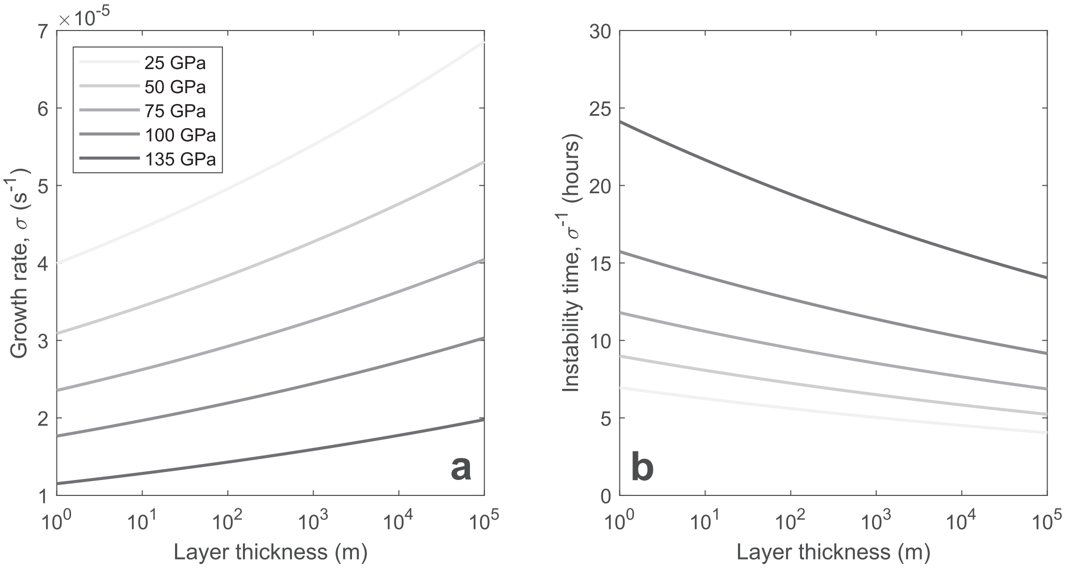

Figure 5. Rayleigh-Taylor instability of a metal layer in a magma ocean. The growth rate (a) and instability time (b) for a mid-mantle metal layer, based on the parameterization of Rayleigh-Taylor instabilities in a spherical geometry by Mondal and Korenaga (2018). A range of thicknesses is shown due to a variety of layer thicknesses proposed (Karato & Murthy, 1997; Rubie et al., 2003; Wood et al., 2006).

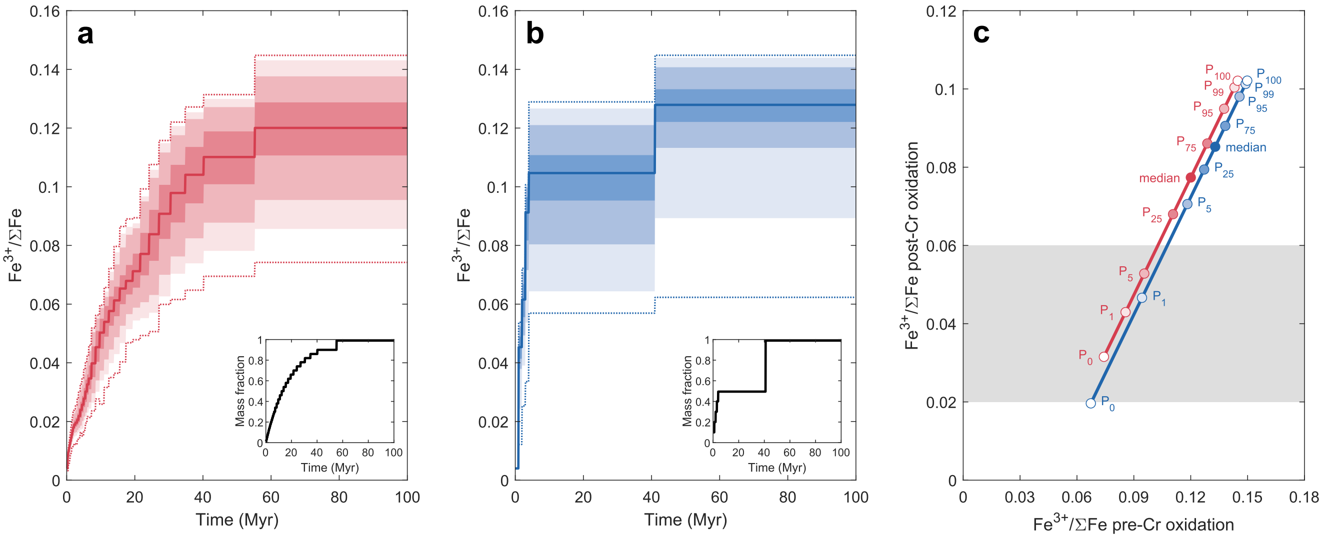

Figure 6. The Fe^{3+}/ΣFe ratio from metal rain in the magma ocean. (a) Results for Monte Carlo sampling on depth of melting and degree of chemical equilibration on mantle Fe^{3+}/ΣFe ratio for discrete impact events using the H04 accretion model (Halliday, 2004) (**inset**) in a magma ocean with constant 3,500 K potential temperature. Dotted lines correspond to the limits of results (0th percentile and 100th percentile). Shading corresponds to 1st–99th percentile (lightest red), 5th–95th percentile, and 25th–75th percentile (darkest red). The 50th percentile (or median) is shown as a solid red line. After each impact, the whole-mantle Fe^{3+}/ΣFe ratio is calculated through convective mixing, thus these values represent bulk-mantle Fe^{3+}/ΣFe. (b) Same as (a), but using the N21 accretion model (Nesvorný et al., 2021) (**inset**). Shading identical, except using blue shades. (c) The final Fe^{3+}/ΣFe ratio at the end of primary accretion from Monte Carlo results (as given in (a) and (b)) before and after the removal of 0.35 wt.% $FeO_{1.5}$ by the oxidation of chromium (Hirschmann, 2022). Red and blue shading identical to (a) and (b), with labels $P_\#$ corresponding to percentiles. The values from (b) are shifted by 0.005 to the right for clarity, as otherwise these lines would overlap. Gray region represents estimates on the present-day Fe^{3+}/ΣFe ratio of the mantle. Note that the median (50th percentile) for both models, once main accretion is complete, is above the estimated range for present-day mantle Fe^{3+}/ΣFe.

$$M_m = M_E - M_c. \tag{11}$$

We follow a strategy similar to Rubie et al. (2011) in modeling the pressure profile of the growing mantle. The average density of the mantle scales linearly with Earth's mass, beginning at 3,400 kg/m^3 (characteristic of upper mantle silicate density):

$$\rho_m = (4500 - 3400)\,F + 3400, \tag{12}$$

where F is the fraction of Earth's mass compared to present. Core density, ρ_c, is determined as $2.5\rho_m$. The pressure at the CMB, P_{cmb}, during accretion is calculated by using Eqn 2.73 of Turcotte and Schubert (2014), assuming a simple two-layer model for a planet:

$$P_{\text{cmb}} = \frac{4}{3}\pi G\rho_m R_c^3(\rho_c - \rho_m)\left(\frac{1}{R_c} - \frac{1}{R_E}\right) + \frac{2}{3}\pi G\rho_m^2\left(R_E^2 - R_c^2\right), \tag{13}$$

where G is the gravitational constant. During the merger of an impactor with a growing Earth, the radius of the core, R_c, the radius of Earth, R_E, and the density of the core, ρ_c, changes, affecting P_{cmb}. Owing to this time-dependent growth during an impactor event, we chose to simplify the calculation of P_{cmb}. As such, we made the following choices to represent the intermediate situation during each accretion event: (i) half the impactor core mass contributes to the calculation of R_c, (ii) all of the impactor silicate contributes to mantle mass and therefore R_E, (iii) the average core density, $\rho_{c,avg}$, is the mean between pre- and post-impact Earth ρ_c and (iv) the impactor is differentiated, with core and mantle masses as described by Rubie et al. (2011) (their Figure 4 and Supplementary Data Tables S3a and S3b; our Table S5 in Supporting Information S1). Note that, although assumption (i) assumes half the impactor core has merged with the core for purposes of calculating R_c, this does not mean that this mass avoids equilibration with the magma ocean. We model the effective impactor core mass equilibrated in a later step. With assumptions (i)–(iv), we calculate the radius of Earth's core during an impact as:

$$R_c = \left[\frac{3}{4\pi}\frac{\left(M_c + \frac{1}{2}M_{c,\text{imp}}\right)}{\rho_{c,\text{avg}}}\right]^{\frac{1}{3}}, \tag{14}$$

where $M_{c,\text{imp}}$ is the mass of the impactor core, and we determine the Earth's overall radius as:

$$R_E = \left[\frac{3}{4\pi}\left(\frac{M_m}{\rho_m} + \frac{M_c + \frac{1}{2}M_{c,\text{imp}}}{\rho_{c,\text{avg}}}\right)\right]^{\frac{1}{3}}. \tag{15}$$

Note, from assumption (ii) above, we use the post-impact M_m and ρ_m. Using Equations 12, 14 and 15, along with the assumptions (i)–(iv) listed above, we determine an approximate P_{cmb} from Equation 13 during an accretion event. This value of P_{cmb} should be taken as a reasonable (although not exact) approximation for the average CMB pressure during an accretion event. The pressure at the bottom of the magma ocean, P_{mo}, is determined by a fraction, f, from P_{cmb}:

$$P_{\text{mo}} = fP_{\text{cmb}}. \tag{16}$$

For simplicity, the depth of a magma ocean is assumed to be constant across the globe even for the case of late accretion where the spatial extent may be regional (Citron & Stewart, 2022; Marchi et al., 2014).

For the composition of the growing Earth, we also follow Rubie et al. (2011) (their Figure 4 and Supplementary Data Tables S3a and S3b; our Table S4 in Supporting Information S1). Their model, however, initiates with a mass fraction of 0.11 for the Earth, but our H04 model initiates at 0.01. For mass fractions between 0.01 and 0.11, we estimate the composition of the proto-Earth by decreasing FeO in the Rubie et al. (2011) composition and compensating it with a corresponding increase in wt. % SiO_2 but keep other compositional components the same.

For impactor mantle composition, we again use the model of Rubie et al. (2011). In this model, impactors are distinguished as "early" or "late" (their Supplementary Data Table S3a; our Table S5 in Supporting Information S1). In the H04 model, "early" impactors occur for an Earth mass fraction less than 0.67. In the N21 model, early impactors occur for an Earth mass fraction less than 0.33 and late impactors between 0.33 and 0.5. This allows us to use an Earth-like composition for the last giant impact, which gives a more reasonable FeO wt. % for the impactor. For simplicity, we keep impactor mantle compositions the same as those given in Rubie et al. (2011), except that we vary FeO based on the additional FeO needed to obtain the next step in FeO wt. % for a growing Earth. As such, impactor FeO wt. % varies through accretion (unlike in the Rubie et al. (2011) model which maintains nearly constant FeO wt. %). We compensate for the differing FeO wt. % by a corresponding change in SiO_2. This change is small, thus still aligning well with the Rubie et al. (2011) composition and f_{O_2}. For the mass of impactor cores, we use the proto-Earth core mass given by Rubie et al. (2011) (their Supplementary Data Table S3b) and use the difference in core mass between accretion steps. For impactor core composition, we maintain the "early" and "late" scheme from Rubie et al. (2011). Impactors' mantle FeO content and core Fe content affects their f_{O_2} (by Equation 4) and hence their $Fe^{3+}/\Sigma Fe$ by Equation 3. We use a median equilibrium pressure and temperature for impactors by Rubie et al. (2011) to obtain oxygen fugacity, and then we solve Equation 3 to determine the corresponding impactor $Fe^{3+}/\Sigma Fe$. For a late accretion impactor, we use Earth-like composition and an equilibrium pressure and temperature given by Rubie et al. (2011) for a 1% Earth mass impactor.

4.2. Equilibration of Metal Droplets

Impactor cores could break up quickly into millimeter- to centimeter-sized droplets in the magma ocean due to Rayleigh-Taylor instabilities (Ichikawa et al., 2010; Qaddah et al., 2019), although estimates on break-up efficiency vary (Dahl & Stevenson, 2010; Deguen et al., 2014; Landeau et al., 2021; Rubie et al., 2003). For droplet size, we adopt 0.5 cm radius, corresponding to efficient break-up. Inefficient break-up is modeled later by changing the degree of equilibration. The mass of a single metal droplet, m_d, is:

$$m_d = \frac{4}{3}\pi r_d^3 \rho_{Fe}, \tag{17}$$

where r_d is droplet radius and ρ_{Fe} is density of liquid iron. The total number of droplets, N_d, from one impactor would be:

$$N_d = \frac{M_{c,\mathrm{imp}}}{m_d}. \tag{18}$$

where $M_{c,\mathrm{imp}}$ is the mass of the impactor. Descending droplets in a magma ocean equilibrate a total amount of silicate mass, ΔM_{eq}, given by:

$$\Delta M_{\mathrm{eq}} = \tau J \kappa N_d. \tag{19}$$

where τ is the equilibration time scale, J is the equilibrated mass flux per droplet, and κ is the degree of equilibration. An equilibration factor, κ, has been adopted by prior studies (Halliday, 2004; Nimmo et al., 2010; Rudge et al., 2010; Zube et al., 2019) to represent the fraction of impactor core which equilibrates with silicate melt. Estimates on core breakup and the degree of equilibration vary from nearly complete breakup and a high degree of equilibration (Deguen et al., 2014) to incomplete breakup and a low degree of equilibration, particularly for large impactors (Dahl & Stevenson, 2010; Landeau et al., 2021). A high degree of equilibration corresponds to where most of an impactor's core fragments and easily equilibrates with silicate, whereas low equilibration corresponds to limited fragmentation or where most of the impactor's core merges directly with the proto-Earth's core.

To determine the mass of equilibrated silicate per unit time, J, we adopt the "droplet" regime for chemical equilibration from Ulvrová et al. (2011). The "droplet" regime is characteristic of a high Reynolds number and low viscosity ratio between liquid iron and silicate melt. In this model, the mass of silicate equilibrated per unit time per droplet can be estimated by the diffusion limited ring around the droplet as it falls, given as:

$$J = 2\pi r_d \left(\frac{h}{2}\right) v_d \rho_{Si}, \tag{20}$$

where ρ_{Si} is silicate melt density (Rubie et al., 2003), v_d is the velocity of droplets, and h is the diffusion boundary. The diffusion boundary thickness is:

$$h = \frac{r_d}{a\mathrm{Pe}^{0.5}}, \tag{21}$$

where $a = 0.79$, and Pe is the Peclet number, calculated as:

$$\mathrm{Pe} = \frac{r_d v_d}{D}. \tag{22}$$

We use a velocity for droplets, v_d, of 0.5 m/s (Rubie et al., 2003) and a chemical diffusivity, D, of 10^{-7} m^2 s^{-1} (Solomatov, 2015). To account for a diffusion gradient, we divide h by two as shown in Equation 20. The equilibration time, τ, is parameterized as (Ulvrová et al., 2011):

$$\tau = \frac{\mathrm{Pe}}{3}\left[\frac{K}{\mathrm{Sh}} + \frac{1}{10R_D}\right]\frac{r_d}{v_d}. \tag{23}$$

In above, we estimate the partition coefficient as $K \sim X_{\mathrm{Fe}}^{\mathrm{metal}}/X_{\mathrm{FeO}}^{\mathrm{silicate}} \sim 10$ (Fischer et al., 2015) and the diffusivity ratio, R_D, as on the order of ∼1. The Sherwood number, Sh, is determined by:

$$\mathrm{Sh} = a\mathrm{Pe}^{0.5}. \tag{24}$$

Combining Equations 20–24 with Equation 19 gives the total silicate mass equilibrated by a given impactor. Note that it is possible for ΔM_{eq} from Equation 19 to be larger than the mass of the magma ocean, M_{mo}, such as during large impactor:proto-Earth accretionary events or shallow magma oceans. If this is the case, we set $\Delta M_{\mathrm{eq}} = M_{\mathrm{mo}}$, therefore assuming the whole magma ocean is equilibrated. Constants and variables used in metal droplets modeling are given in Table S3 in Supporting Information S1.

For our Monte Carlo sampling scheme, at each impact, we randomly select the degree of equilibration ($0 \le \kappa \le 1$) and the depth of the magma ocean ($0 \le f \le 1$). We assume the minimum possible depth of the magma ocean would be if only the impactor melted ($f = 0$) and the maximum possible depth of the magma ocean would be to the proto-Earth CMB ($f = 1$). We vary the depth of the magma ocean because accretionary impacts may not melt the entire mantle (Nakajima et al., 2021). Although smaller impactor:proto-Earth mass ratios would have less melting potential compared to larger impactors, we did not adjust f accordingly owing to the uncertainties involved in accretionary impact dynamics. Any possible correlations between impactor mass and melting would be within our Monte Carlo sampling. For the P-T conditions of the magma ocean, we choose the 3,500 K potential temperature adiabat (Figure 2a). The main text reports results using 3,500 K, but we also test where mantle potential temperature is determined by where P_{mo} crosses the liquidus (Figures S1–S3 and S4c–S4d in Supporting Information S1).

At each impact, we first mix the impactor mantle with Earth's magma ocean and determine the change in $\mathrm{Fe}^{3+}/\Sigma\mathrm{Fe}$ in the magma ocean prior to equilibration:

$$\Delta r = \frac{M_{\mathrm{FeO,imp}}}{M_{\mathrm{FeO,imp}} + M_{\mathrm{FeO,mo}}}(r_{\mathrm{imp}} - r_{\mathrm{mo}}), \tag{25}$$

where $M_{\mathrm{FeO,imp}}$ and r_{imp} are mass of FeO and the $\mathrm{Fe}^{3+}/\Sigma\mathrm{Fe}$ of the impactor mantle, respectively, and $M_{\mathrm{FeO,mo}}$ and r_{mo} is the FeO and the $\mathrm{Fe}^{3+}/\Sigma\mathrm{Fe}$ in the melted portion of Earth's, respectively. We initiate Earth $\mathrm{Fe}^{3+}/\Sigma\mathrm{Fe}$ as 0.004

for the first impact, but for subsequent impacts, r_{mo} is the final $\mathrm{Fe}^{3+}/\Sigma\mathrm{Fe}$ determined from the equilibration of the previous impact.

Then, we determine the equilibrium $\mathrm{Fe}^{3+}/\Sigma\mathrm{Fe}$ as a function of temperature, pressure, and composition (Equation 3). As $\mathrm{Fe}^{3+}/\Sigma\mathrm{Fe}$ is pressure- and temperature-dependent (Figure 2b), we subdivide the magma ocean into layers with a pressure increment of 0.5 GPa. As droplets fall, they equilibrate an amount of silicate ΔM_{eq} and buffer its $\mathrm{Fe}^{3+}/\Sigma\mathrm{Fe}$ by a given ΔIW from composition (Equation 4). At each pressure increment, i, the $\mathrm{Fe}^{3+}/\Sigma\mathrm{Fe}$ of the magma ocean would change as:

$$\Delta r = \frac{\Delta M_{\mathrm{eq}}}{M_{\mathrm{mo}}}\left(r_{\mathrm{eq},i} - r_{\mathrm{mo}}\right), \tag{26}$$

where $r_{\mathrm{eq},i}$ is the $\mathrm{Fe}^{3+}/\Sigma\mathrm{Fe}$ equilibrated value at the P-T conditions. This equilibration and mixing continues through the magma ocean to P_{mo}. It would take droplets approximately 70 days at a velocity of 0.5 m s^{-1} to reach the present-day CMB, and less time in a still accreting Earth. Compared to the time scale of accretion (millions of years), the $\mathrm{Fe}^{3+}/\Sigma\mathrm{Fe}$ ratio in the magma ocean changes on very short time scales. For ease of computation, after each impact, we determine the change in final whole-mantle ratio assuming convective mixing, thus leaving no redox zonation in the mantle between impacts by:

$$\Delta r = \frac{M_{\mathrm{FeO,mo}}}{M_{\mathrm{FeO,mo}} + M_{\mathrm{FeO},m}}\left(r_{\mathrm{mo}} - r_0\right), \tag{27}$$

where $M_{\mathrm{FeO},m}$ and r_0 are mass of FeO and the $\mathrm{Fe}^{3+}/\Sigma\mathrm{Fe}$ of the underlying un-melted mantle, respectively. The $\mathrm{Fe}^{3+}/\Sigma\mathrm{Fe}$ of the whole mantle after an impact is subsequently used for r_{mo} in Equation 25 and r_0 in Equation 27 for the next impact. Upon magma ocean solidification, as much as 0.35 wt.% Fe^{3+} is reduced to Fe^{2+} by electron exchange with Cr^{2+} (Hirschmann, 2022) (Figure 2b, gray shading). We incorporate this effect after the last giant impact (Figure 6c).

4.3. Changes in Mantle $\mathrm{Fe}^{3+}/\Sigma\mathrm{Fe}$ Throughout Accretion

Using the Monte Carlo sampling scheme described above, our results indicate that the likely range (5th–95th percentiles) of mantle $\mathrm{Fe}^{3+}/\Sigma\mathrm{Fe}$, after Cr oxidation, is between 0.053 and 0.095 or 0.071 to 0.098, for the H04 and N21 models, respectively (Figure 6). The present-day mantle $\mathrm{Fe}^{3+}/\Sigma\mathrm{Fe}$ is estimated to be between 0.02 and 0.06 (Frost & McCammon, 2009; Hirschmann, 2022). Neither model reproduces this range at the 50th percentile (median) and only the lowest percentiles are satisfactory, suggesting that either low degrees of equilibration or shallow magma oceans are required. Studies have used mantle Hf-W and U-Pb isotopic signatures to constrain the degree of equilibration to at least 30%, and depending on the timing of core formation, upwards of 70% (Halliday, 2004; Nimmo et al., 2010; Rudge et al., 2010; Zube et al., 2019). Our results suggest that obtaining present-day $\mathrm{Fe}^{3+}/\Sigma\mathrm{Fe}$ is unlikely with such higher degrees of equilibration. We also vary κ and f continuously through all of accretion (Figure S4 in Supporting Information S1) and similarly obtain a rather narrow range of possible degrees of equilibration and depths of magma ocean. Below, we show that variability in equilibration for the last giant impact can reconcile mantle oxidation and isotope systematics by forming mantle redox stratification.

5. Consequences of the Last Giant Impact and Late Accretion

Simply by its size, the last giant impact has significant potential for mantle equilibration, and, after the last giant impact, the average oxidation state of the whole mantle would remain largely stable. If metal efficiently equilibrated in a deep magma ocean, the resulting $\mathrm{Fe}^{3+}/\Sigma\mathrm{Fe}$ would be high (~0.15) (Figure 2b). As the amount of mantle melting depends on impact dynamics (Nakajima et al., 2021), it is possible that the last giant impact melted and equilibrated only some of the mantle, leaving the lower (un-melted) part of the mantle with its former oxidation state. To determine the range of possible $\mathrm{Fe}^{3+}/\Sigma\mathrm{Fe}$ of the mantle after the last giant impact, we varied the depth and degree of equilibration continuously for the last giant impact (Figure 7, color contours). We also determined the whole-mantle average $\mathrm{Fe}^{3+}/\Sigma\mathrm{Fe}$ (by Equation 27) to show depths and degrees of equilibration that could reproduce the present-day bulk mantle $\mathrm{Fe}^{3+}/\Sigma\mathrm{Fe}$ after convective mixing (Figure 7, gray shading). Our results show that equilibration of the last giant impact is no longer necessarily limited to low degrees of

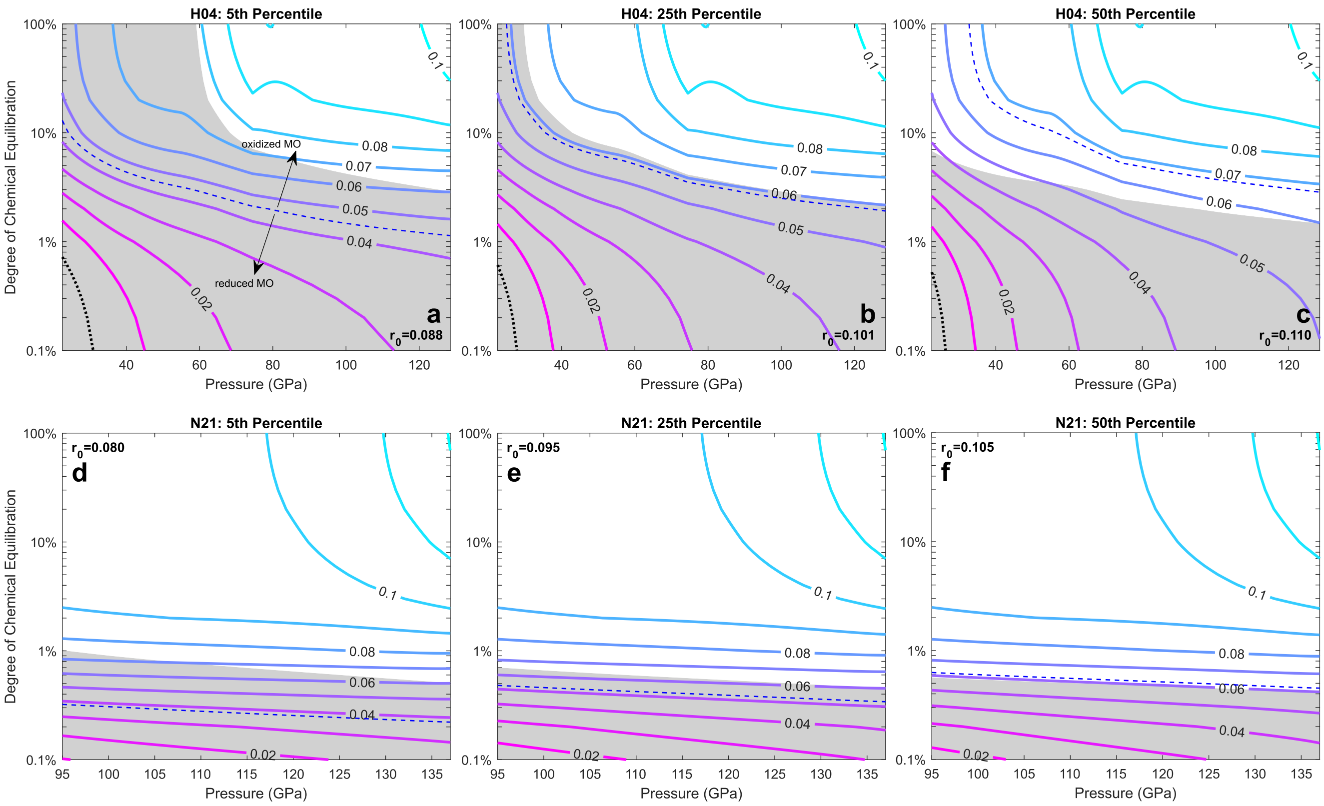

Figure 7. The $Fe^{3+}/\Sigma Fe$ ratio of a magma ocean after the last giant impact. Contours for the $Fe^{3+}/\Sigma Fe$ ratio of a magma ocean after a Moon-forming giant impact (1:10 impactor:proto-Earth mass ratio labeled H04 (Halliday, 2004) (a–c), and 1:1 impactor:proto-Earth mass ratio labeled N21 (Nesvorný et al., 2021) (d–f) as a function of magma ocean depth and degree of chemical equilibration. Initial whole-mantle $Fe^{3+}/\Sigma Fe$ ratios (r_0) correspond to the 5th, 25th, and 50th percentile of Monte Carlo sampling before the last giant impact, at 55 and 41 Myr for their respective models (Figures 6a and 6b). The value r_0 is given prior to Cr oxidation, whereas the contour $Fe^{3+}/\Sigma Fe$ values are corrected for the effect of Cr oxidation. The black dotted contours represent where $Fe^{3+}/\Sigma Fe = 0$ because of this effect. The blue dashed line delineates redox stratification between magma ocean and underlying mantle, where the magma ocean is either more oxidized or more reduced (demonstrated by arrows in (a)). Gray shading corresponds to the pressures and degrees of equilibration where the resulting whole-mantle $Fe^{3+}/\Sigma Fe$ after convective mixing replicates modern-day estimates.

equilibration or shallow depths. In the H04 model, with an initial $Fe^{3+}/\Sigma Fe$ ratio of 0.088 and 0.101 (5th and 25th percentiles prior to the last giant impact), the present-day oxidation state can be achieved by a magma ocean up to a depth of about 40 GPa with any degree of equilibration (Figures 7a and 7b). Alternatively, a low degree of equilibration at any depth also reproduces present-day mantle redox when the $Fe^{3+}/\Sigma Fe$ ratio before the last giant impact is <0.11 (Figure 7c). Beyond an initial $Fe^{3+}/\Sigma Fe$ ratio of ~0.11 prior to the last giant impact, the H04 model cannot reproduce mantle oxidation state, indicating an upper bound to initial $Fe^{3+}/\Sigma Fe$. The N21 model necessitates low degrees of equilibration (<1%) for the last giant impact but is not so limited in depth (Figures 7d–7f). It should be noted that our modeling of N21 assumes all metal accretes at once, which may be unrealistic given the dynamics of a 1:1 mass ratio collision (Canup, 2012). As such, the N21 model should be treated as an end-member case.

The last giant impact is the final opportunity to modify or reset mantle redox through magma ocean equilibration. Thus, if the last giant impact does not melt the whole mantle, stratification in terms of $Fe^{3+}/\Sigma Fe$ occurs. The underlying (un-melted) mantle maintains its former $Fe^{3+}/\Sigma Fe$ from prior accretion events. In both models, our Monte Carlo results show that earlier impactors likely left a much too oxidized mantle $Fe^{3+}/\Sigma Fe$ (greater than 0.10 before the last giant impact; Figures 6a and 6b). To reconcile mantle $Fe^{3+}/\Sigma Fe$, the last giant impact likely left a more reduced magma ocean (Figure 7, blue dashed lines). There is the possibility that the last giant impact left a more oxidized upper mantle (e.g., Figure 7a, gray shading above blue dashed line), but this only occurs within the lower bounds of our Monte Carlo sampling (<5th percentile).

In the H04 model, the degree of equilibration required by Hf-W and U-Pb systematics (30%–70%) (Halliday, 2004; Nimmo et al., 2010; Rudge et al., 2010; Zube et al., 2019) necessitates a mid-mantle depth for the magma ocean by the last giant impact to reproduce present-day mantle $Fe^{3+}/\Sigma Fe$. The last giant impact in the N21 model cannot equilibrate at such high efficiencies without leaving the mantle much too oxidized (Figures 7d–7f). An alternative scenario is that accretion prior to the last giant impact was highly efficient, and the last giant impact equilibrated much less efficiently, thereby leading to an average equilibration of 30%–70% through all of accretion (see also Figure S4 in Supporting Information S1). Our results demonstrate this possibility by the broad range of permitted regions for magma ocean depth when equilibration is low (<10%) for the last giant impact (all of Figure 7). Low degrees of equilibration represent a scenario where the impactor core fragmented very little or merged quickly with the proto-Earth's core. Whole-mantle melting avoids redox stratification, but this would limit the dynamics of the last giant impact to processes leading to low equilibration.

Redox stratification could also occur with late accretion impacts. Late accretion would involve smaller impactors (though potentially up to 3,000 km in diameter) that could have melted fractions of the upper mantle (Korenaga & Marchi, 2023; Marchi et al., 2014, 2018) and equilibrated to produce a more reduced upper mantle. To explore the effects of such a late accretion impact, we chose the post-giant impact 1st, 5th, 25th, and 50th percentiles of the H04 model from our Monte Carlo sampling and varied the depth of melting and degree of equilibration for a 1% Earth mass impactor (Genda et al., 2017; Marchi et al., 2018). We limit the depth of melting to 50 GPa (~1,200 km depth), owing to relatively shallow melting potential for late accretion impactors (Korenaga & Marchi, 2023; Marchi et al., 2018). The impactor could drop upper mantle $Fe^{3+}/\Sigma Fe$ to as low as 0.01, and the formation of a more reduced magma ocean compared to the underlying mantle is likely (Figures 8a and 8b). In contrast to the last giant impact, if the mantle $Fe^{3+}/\Sigma Fe$ started too high (>0.06), a late accretion impactor may not be able to reconcile the bulk mantle $Fe^{3+}/\Sigma Fe$ (Figures 8c and 8d).

6. Discussion

Despite the stochastic nature of impact dynamics, our results indicate that the mantle after primary accretion is likely to have been oxidized too strongly ($Fe^{3+}/\Sigma Fe > 0.06$) (Figure 6). There is a relatively low probability through the whole of accretion (below the median of Monte Carlo sampling) for Earth to assume its present-day bulk mantle $Fe^{3+}/\Sigma Fe$. The degree of metal-silicate equilibration inferred from Hf-W and U-Pb systematics (Halliday, 2004; Nimmo et al., 2010; Rudge et al., 2010; Zube et al., 2019) requires a very narrow range of magma ocean depths (Figure S4 in Supporting Information S1) or such equilibration would lead to too high $Fe^{3+}/\Sigma Fe$. Our results suggest that the mantle oxidation state provides an important constraint on accretion scenarios. Although the details of the last giant impact remain elusive, its dynamics would largely determine the final redox state of the mantle. In the models we tested, the last giant impact may either equilibrate in a relatively shallow magma ocean with any degree of equilibration or at any magma ocean depth with a very low degree of equilibration. Prior studies have determined that metal-silicate equilibrium must be established at an effective pressure in the mid-mantle to explain the abundance of moderately siderophile elements (Fischer et al., 2015), and therefore metal droplets must have equilibrated at this effective pressure to explain the oxidation state of the mantle. This provides additional evidence that the last giant impact may not have melted the whole mantle, thereby imprinting redox stratification.

The dynamics of the last giant impact and late accretion would also affect the abundance of highly siderophile elements (HSEs) in the mantle. Most attribute HSE abundance to accretion after the last giant impact and core formation (Morbidelli & Wood, 2015), but the Moon-forming impactor (Theia) itself could account for HSEs in the mantle. Sleep (2016) estimated that $2.3–10 \times 10^{21}$ kg of Fe in the Earth's mantle could have come from Theia's core and was subsequently oxidized through the reactions $Fe_2O_3 + Fe \rightarrow 3FeO$ and $Fe + H_2O \rightarrow FeO + H_2$. Assuming that all the Fe was oxidized by reduction of Fe_2O_3 in the mantle, then approximately $2.2–9.5 \times 10^{21}$ kg of Fe_2O_3 could have been reduced. In an Earth mantle with 8 wt.% FeO*, this would result in a drop in $Fe^{3+}/\Sigma Fe$ between 0.007 and 0.030. If the bulk of Theia's core first equilibrated in a deep magma ocean, leaving a highly oxidized mantle ($Fe^{3+}/\Sigma Fe >$ s0.10), and a later "Theian core veneer" (as proposed by Sleep (2016)) was oxidized in a shallower magma ocean where equilibrium $Fe^{3+}/\Sigma Fe$ was lower (see Figure 2), then this drop in overall mantle $Fe^{3+}/\Sigma Fe$ may be able to account for present-day mantle oxidation state. If water was the main oxidant instead, the decrease in $Fe^{3+}/\Sigma Fe$ may be too small to reconcile mantle oxidation state. Sleep (2016) proposed this model to contrast a late veneer addition of HSEs, but this model depends critically on the dynamics of the last giant impact and the behavior of the lunar disk, both of which are not well understood (Canup et al., 2023). Two

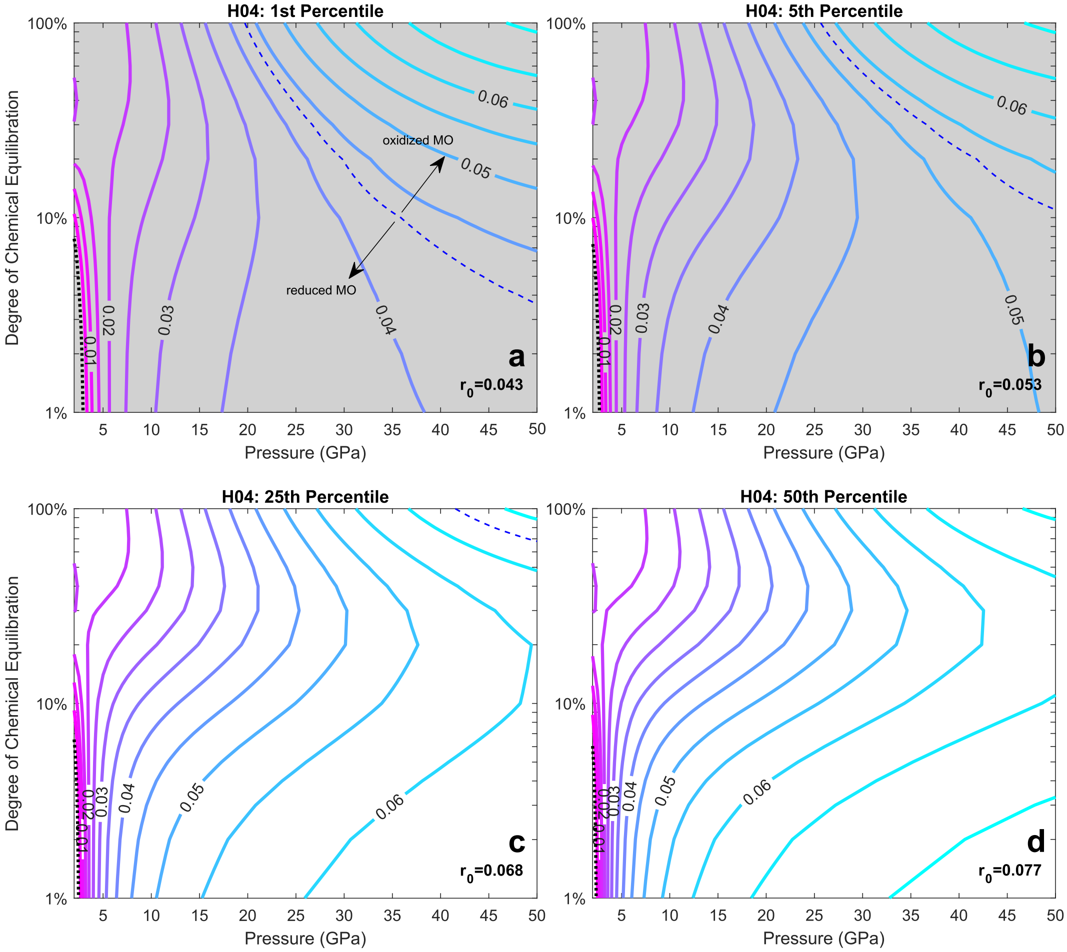

Figure 8. Contours for the $Fe^{3+}/\Sigma Fe$ ratio from a large late accretion impact (1% present-day Earth mass) in a magma ocean with a 3500 K potential temperature. The initial mantle $Fe^{3+}/\Sigma Fe$ ratio (r_0) corresponds to the 1st, 5th, 25th, and 50th percentiles for the H04 (Halliday, 2004) model (a–d, respectively). Both r_0 values and contours have been corrected for Cr oxidation. Gray shading corresponds to regions which replicate the present-day estimates for mantle $Fe^{3+}/\Sigma Fe$ after whole-mantle convective mixing. The blue dashed line delineates the contour for redox stratification, where the magma ocean is either more reduced or more oxidized than underlying mantle (demonstrated by arrows in (a)). The dotted black line delineates regions with $Fe^{3+}/\Sigma Fe = 0$. Note that in both (c) and (d), the final $Fe^{3+}/\Sigma Fe$ after mixing remains above present-day estimates for all efficiencies and depths shown. Although the N21 accretion model is not shown, one can infer by comparison using Figure 6c (e.g., the 5th percentile value of N21 is close to 25th percentile of H04, and thus would be similar to (c)).

alternate explanations could explain mantle HSE abundance without resolving the details of the Moon-forming giant impact: the capture of metal in a partially molten mantle layer resulting from a late accretion impact (Korenaga & Marchi, 2023) and a tendency toward lithophile behavior of HSEs at high pressure and temperature conditions (Suer et al., 2021), though the latter explanation may not be able to explain the chondritic relative abundance of HSEs. The metal-capture explanation implies that the eventual mixing of captured metallic Fe with the mantle helps reduce the mantle $Fe^{3+}/\Sigma Fe$, as in the model of Sleep (2016), but because this convective mixing takes place over Earth history (Korenaga & Marchi, 2023), its reducing efficacy has to be evaluated with other redox-relevant, long-term geological processes such as the subduction of oxidized oceanic crust (Kasting et al., 1993; Lécuyer & Ricard, 1999; Nicklas et al., 2019).

More importantly, both the last giant impact and late accretion impacts would result in an initially stratified oxidation state for the mantle, but to different degrees. A large late accretion impact would produce localized regions of upper mantle that are highly reduced. Outgassing of such regions would include reduced species, such as CO, CH_4, and H_2 (Gaillard et al., 2022; Hirschmann, 2012), producing a surface environment that is favorable for the synthesis of biomolecules (Benner et al., 2020; McCollom, 2013). Prior studies have suggested a possibility to create a reducing environment from impactor core interactions with surface water (Itcovitz et al., 2022; Zahnle et al., 2020), but these studies rely on having at least one ocean mass of water available and that the metal remains on the surface. The amount of available surface water during the early Hadean is likely limited, as water is mostly trapped in a solidifying magma ocean (Miyazaki & Korenaga, 2022; Salvador & Samuel, 2023). Also, metal from impacts is largely incorporated directly into the solid part of the mantle or the core (Korenaga & Marchi, 2023). Our analysis shows that it is possible to create a reducing surface environment from late accretion impacts, without relying on the presence of a voluminous water ocean or the availability of impactor metal at the surface.

The Moon-forming impact was likely the last significant impact that could have melted substantial portions of the mantle and therefore reset mantle composition and redox. Without whole-mantle melting, redox stratification by the last giant impact is inevitable because underlying, un-melted mantle would maintain its former redox state. If the last giant impact produced a more reduced upper mantle, solid mantle convection over long time scales would bring up more oxidized material from depth. This would increase upper mantle f_{O_2} and outgas less reduced volcanic gases (Hirschmann, 2023; O'Neill & Aulbach, 2022). Recent studies have shown that the mantle may have been more reduced in the Archean (Aulbach & Stagno, 2016; Nicklas et al., 2019), indicating a secular change in mantle redox. If mantle outgassing became more oxidized with time, the overall atmospheric composition would change, potentially allowing for the accumulation of oxygen. The change in upper mantle redox has been hypothesized as a factor in regulating oxygen accumulation in Earth's atmosphere over geologic time (Andrault et al., 2018; Aulbach & Stagno, 2016; Kasting et al., 1993; Kump et al., 2001; Lécuyer & Ricard, 1999; O'Neill & Aulbach, 2022), such as the Great Oxidation Event (GOE) at 2.4 Ga when atmospheric oxygen increased by several orders of magnitude (Lyons et al., 2014).

So far, most studies have used the disproportionation of FeO in bridgmanite or silicate melt at higher temperatures and pressures to explain pre-existing mantle redox heterogeneity (Figure 2b). Whereas disproportionation in bridgmanite may produce Fe metal and enriched Fe^{3+} silicate, a net change in oxidation occurs only by the removal of the metal (Hirschmann, 2022). Percolation of metal in lower mantle minerals, however, is unlikely to be efficient (Rubie et al., 2015). In contrast, removal of Fe metal in silicate occurs quickly in the melt phase, but any heterogeneity is erased due to rapid convective mixing in magma oceans (Solomatov, 2015). It is through repeated melting and solidification of the mantle during stochastic accretion, as proposed in this study, that any redox heterogeneity can remain long-term. Convective mixing of this solid, heterogenous mantle could then take place over billions of years, therefore changing upper mantle f_{O_2} and playing a role in the atmosphere's oxygenation (O'Neill & Aulbach, 2022). Another proposed mechanism for an increase in upper mantle f_{O_2} is through subduction of relatively oxidized oceanic crust, but this effect has been found to be too small to explain modern-day mantle oxidation state (Kasting et al., 1993; Lécuyer & Ricard, 1999; Nicklas et al., 2019). Additionally, if plate tectonics occurred in the Hadean and Archean, when the mantle was hotter, much of this oxidized material could have been recycled back into the lithosphere (Kelemen & Behn, 2016). As such, the ability for subduction to oxidize the upper mantle through deep time is unclear.

Other studies have found no secular change in upper mantle f_{O_2} since at least the Archean (Canil, 2002; F. Zhang, Stagno, et al., 2024). This could indicate that any mantle redox stratification left behind by the last giant impact was either minor or was homogenized by at least the Archean. Another possibility is that the last giant impact left behind a more oxidized upper mantle (Figure 7), This would require a more reduced proto-Earth mantle before the Moon-forming impact, created by either equilibration at low efficiencies or in shallow magma oceans (Figure 6). These conditions are difficult given our Monte Carlo sampling results.

Our results indicate that equilibration by a metal layer tends towards lower mantle $Fe^{3+}/\Sigma Fe$ than presently observed (0.02–0.06), while equilibration by fragmentation of impactor cores (metal droplets) tends to a higher mantle $Fe^{3+}/\Sigma Fe$. Although both mechanisms operated during Earth formation (Figure 1), equilibration by metal droplets was the most efficient mechanism and thereby determined the final redox state of the mantle. Without whole-mantle melting, the final stages of accretion (the Moon-forming giant impact and late accretion) resulted in redox stratification. Other studies have proposed various mechanisms to produce mantle redox stratification in the early Earth mantle (Nicklas et al., 2019; O'Neill & Aulbach, 2022; Zahnle et al., 2020), but we suggest that redox stratification is a natural consequence of accretion. Additionally, to reproduce the present-day bulk mantle redox, the Moon-forming giant impact likely did not melt the whole mantle, consistent with metal-silicate equilibration of moderately siderophile elements (Fischer et al., 2015). Resulting mantle redox stratification would influence the subsequent geochemical and geophysical evolution for the Earth. As prebiotic chemistry likely requires a relatively reducing environment (McCollom, 2013), degassing from a reducing mantle may be an important component in the emergence of life. As such, it is important to consider a planet's accretionary history for habitability and the emergence of life. The stochasticity of impacts during accretion could lead to divergent oxidation states for the mantles of Earth-like planets, and further effect their surface environments in the short and long term.

Data Availability Statement

Software Availability Statement: The magma ocean redox evolution modeling code presented in this paper is archived on Zenodo (Henningsen, 2024). The archive includes all input files needed to run MATLAB simulations, as well as the simulation output results for Figures 2–8, Figures S1–S4 in Supporting Information S1.

Acknowledgments
The authors thank two anonymous reviewers for their thorough and constructive comments. This work is supported in part by the U.S. National Science Foundation Grants EAR-2102777 and EAR-2102571 and the U.S. National Aeronautics and Space Administration under Cooperative Agreement No. 80NSSC19M0069 issued through the Science Mission Directorate.

References

Abe, Y. (1993). Physical state of the very early Earth. *Lithos*, *30*(3–4), 223–235. https://doi.org/10.1016/0024-4937(93)90037-D

Andrault, D., Muñoz, M., Pesce, G., Cerantola, V., Chumakov, A., Kantor, I., et al. (2018). Large oxygen excess in the primitive mantle could be the source of the Great Oxygenation Event. *Geochemical Perspectives Letters*, *6*(6), 5–10. https://doi.org/10.7185/geochemlet.1801

Armstrong, K., Frost, D. J., McCammon, C. A., Rubie, D. C., & Boffa Ballaran, T. (2019). Deep magma ocean formation set the oxidation state of Earth's mantle. *Science*, *365*(6456), 903–906. https://doi.org/10.1126/science.aax8376

Aulbach, S., & Stagno, V. (2016). Evidence for a reducing Archean ambient mantle and its effects on the carbon cycle. *Geology*, *44*(9), 751–754. https://doi.org/10.1130/g38070.1

Barboni, M., Boehnke, P., Keller, B., Kohl, I. E., Schoene, B., Young, E. D., & McKeegan, K. D. (2017). Early formation of the Moon 4.51 billion years ago. *Science Advances*, *3*(1), e1602365. https://doi.org/10.1126/sciadv.1602365

Benner, S. A., Bell, E. A., Biondi, E., Brasser, R., Carell, T., Kim, H. J., et al. (2020). When did life likely emerge on Earth in an RNA-first process? *ChemSystemsChem*, *2*(2), e1900035. https://doi.org/10.1002/syst.201900035

Borg, L. E., Gaffney, A. M., & Shearer, C. K. (2015). A review of lunar chronology revealing a preponderance of 4.34–4.37 Ga ages. *Meteoritics & Planetary Sciences*, *50*(4), 715–732. https://doi.org/10.1111/maps.12373

Boukaré, C. E., Parmentier, E. M., & Parman, S. W. (2018). Timing of mantle overturn during magma ocean solidification. *Earth and Planetary Science Letters*, *491*, 216–225. https://doi.org/10.1016/j.epsl.2018.03.037

Campbell, A. J., Danielson, L., Righter, K., Seagle, C. T., Wang, Y., & Prakapenka, V. B. (2009). High pressure effects on the iron–iron oxide and nickel–nickel oxide oxygen fugacity buffers. *Earth and Planetary Science Letters*, *286*(3–4), 556–564. https://doi.org/10.1016/j.epsl.2009.07.022

Canil, D. (2002). Vanadium in peridotites, mantle redox and tectonic environments: Archean to present. *Earth and Planetary Science Letters*, *195*(1–2), 75–90. https://doi.org/10.1016/S0012-821X(01)00582-9

Canup, R. M. (2012). Forming a Moon with an Earth-like composition via a giant impact. *Science*, *338*(6110), 1052–1055. https://doi.org/10.1126/science.1226073

Canup, R. M., Righter, K., Dauphas, N., Pahlevan, K., Ćuk, M., Lock, S. J., et al. (2023). Origin of the Moon. *Reviews in Mineralogy and Geochemistry*, *89*(1), 53–102. https://doi.org/10.2138/rmg.2023.89.02

Citron, R. I., & Stewart, S. T. (2022). Large impacts onto the early Earth: Planetary sterilization and iron delivery. *The Planetary Science Journal*, *3*(5), 116. https://doi.org/10.3847/PSJ/ac66e8

Dahl, T. W., & Stevenson, D. J. (2010). Turbulent mixing of metal and silicate during planet accretion—And interpretation of the Hf–W chronometer. *Earth and Planetary Science Letters*, *295*(1–2), 177–186. https://doi.org/10.1016/j.epsl.2010.03.038

Deguen, R., Landeau, M., & Olson, P. (2014). Turbulent metal–silicate mixing, fragmentation, and equilibration in magma oceans. *Earth and Planetary Science Letters*, *391*, 274–287. https://doi.org/10.1016/j.epsl.2014.02.007

Deng, J., Du, Z., Karki, B. B., Ghosh, D. B., & Lee, K. K. M. (2020). A magma ocean origin to divergent redox evolutions of rocky planetary bodies and early atmospheres. *Nature Communications*, *11*(1), 2007. https://doi.org/10.1038/s41467-020-15757-0

de Wijs, G. A., Kresse, G., Vocadlo, L., Dobson, D., Alfe, D., Gillan, M. J., & Price, G. D. (1998). The viscosity of liquid iron at the physical conditions of the Earth's core. *Nature*, *392*(6678), 805–807. https://doi.org/10.1038/33905

Dziewonski, A. M., & Anderson, D. L. (1981). Preliminary reference Earth model. *Physics of the Earth and Planetary Interiors*, *25*(4), 297–356. https://doi.org/10.1016/0031-9201(81)90046-7

Fischer, R. A., Nakajima, Y., Campbell, A. J., Frost, D. J., Harries, D., Langenhorst, F., et al. (2015). High pressure metal–silicate partitioning of Ni, Co, V, Cr, Si, and O. *Geochimica et Cosmochimica Acta*, *167*, 177–194. https://doi.org/10.1016/j.gca.2015.06.026

Frost, D. J., Mann, U., Asahara, Y., & Rubie, D. C. (2008). The redox state of the mantle during and just after core formation. *Philosophical Transactions Royal Society Mathematical Physical and Engineering Sciences*, *366*(1883), 4315–4337. https://doi.org/10.1098/rsta.2008.0147

Frost, D. J., & McCammon, C. A. (2008). The redox state of Earth's mantle. *Annual Review of Earth and Planetary Sciences*, *36*(1), 389–420. https://doi.org/10.1146/annurev.earth.36.031207.124322

Frost, D. J., & McCammon, C. A. (2009). The effect of oxygen fugacity on the olivine to wadsleyite transformation: Implications for remote sensing of mantle redox state at the 410 km seismic discontinuity. *American Mineralogist*, *94*(7), 872–882. https://doi.org/10.2138/am.2009.3094

Gaillard, F., Bernadou, F., Roskosz, M., Bouhifd, M. A., Marrocchi, Y., Iacono-Marziano, G., et al. (2022). Redox controls during magma ocean degassing. *Earth and Planetary Science Letters*, *577*, 117255. https://doi.org/10.1016/j.epsl.2021.117255

Genda, H., Brasser, R., & Mojzsis, S. J. (2017). The terrestrial late veneer from core disruption of a lunar-sized impactor. *Earth and Planetary Science Letters*, *480*, 25–32. https://doi.org/10.1016/j.epsl.2017.09.041

Halliday, A. N. (2004). Mixing, volatile loss and compositional change during impact-driven accretion of the Earth. *Nature*, *427*(6974), 505–509. https://doi.org/10.1038/nature02275

Halliday, A. N., & Canup, R. M. (2023). The accretion of planet Earth. *Nature Reviews Earth and Environment*, *4*(1), 19–35. https://doi.org/10.1038/s43017-022-00370-0

Henningsen, E. L. (2024). MOredox23 [Software]. *Zenodo*. https://doi.org/10.5281/zenodo.14837480

Hirschmann, M. M. (2012). Magma ocean influence on early atmosphere mass and composition. *Earth and Planetary Science Letters*, *341–344*, 48–57. https://doi.org/10.1016/j.epsl.2012.06.015

Hirschmann, M. M. (2021). Iron-wüstite revisited: A revised calibration accounting for variable stoichiometry and the effects of pressure. *Geochimica et Cosmochimica Acta*, *313*, 74–84. https://doi.org/10.1016/j.gca.2021.08.039

Hirschmann, M. M. (2022). Magma oceans, iron and chromium redox, and the origin of comparatively oxidized planetary mantles. *Geochimica et Cosmochimica Acta*, *328*, 221–241. https://doi.org/10.1016/j.gca.2022.04.005

Hirschmann, M. M. (2023). The deep Earth oxygen cycle: Mass balance considerations on the origin and evolution of mantle and surface oxidative reservoirs. *Earth and Planetary Science Letters*, *619*, 118311. https://doi.org/10.1016/j.epsl.2023.118311

Ichikawa, H., Labrosse, S., & Kurita, K. (2010). Direct numerical simulation of an iron rain in the magma ocean. *Journal of Geophysical Research*, *115*(B1), B01404. https://doi.org/10.1029/2009jb006427

Itcovitz, J. P., Rae, A. S. P., Citron, R. I., Stewart, S. T., Sinclair, C. A., Rimmer, P. B., & Shorttle, O. (2022). Reduced atmospheres of post-impact worlds: The early Earth. *The Planetary Science Journal*, *3*(115), 115. https://doi.org/10.3847/PSJ/ac67a9

Karato, S., & Murthy, V. R. (1997). Core formation and chemical equilibrium in the Earth: I. Physical considerations. *Physics of the Earth and Planetary Interiors*, *100*(1–4), 61–79. https://doi.org/10.1016/S0031-9201(96)03232-3

Kasting, J. F., Eggler, D. H., & Raeburn, S. P. (1993). Mantle redox evolution and the oxidation state of the archean atmosphere. *The Journal of Geology*, *101*(2), 245–257. https://doi.org/10.1086/648219

Kelemen, P. B., & Behn, M. D. (2016). Formation of lower continental crust by relamination of buoyant arc lavas and plutons. *Nature Geoscience*, *9*(3), 197–205. https://doi.org/10.1038/ngeo2662

Kleine, T., Touboul, M., Bourdon, B., Nimmo, F., Mezger, K., Palme, H., et al. (2009). Hf–W chronology of the accretion and early evolution of asteroids and terrestrial planets. *Geochimica et Cosmochimica Acta*, *73*(17), 5150–5188. https://doi.org/10.1016/j.gca.2008.11.047

Korenaga, J. (2023). Rapid solidification of Earth's magma ocean limits early lunar recession. *Icarus*, *400*, 115564. https://doi.org/10.1016/j.icarus.2023.115564

Korenaga, J., & Marchi, S. (2023). Vestiges of impact-driven three-phase mixing in the chemistry and structure of Earth's mantle. *Proceedings of the National Academy of Sciences of the United States of America*, *120*(43), e2309181120. https://doi.org/10.1073/pnas.2309181120

Kump, L. R., Kasting, J. F., & Barley, M. E. (2001). Rise of atmospheric oxygen and the "upside-dow" Archean mantle. *Geochemistry, Geophysics, Geosystems*, *2*(1), 2000GC000114. https://doi.org/10.1029/2000GC000114

Landeau, M., Deguen, R., Phillips, D., Neufeld, J. A., Lherm, V., & Dalziel, S. B. (2021). Metal-silicate mixing by large Earth-forming impacts. *Earth and Planetary Science Letters*, *564*, 116888. https://doi.org/10.1016/j.epsl.2021.116888

Lécuyer, C., & Ricard, Y. (1999). Long-term fluxes and budget of ferric iron: Implication for the redox states of the Earth's mantle and atmosphere. *Earth and Planetary Science Letters*, *165*(2), 197–211. https://doi.org/10.1016/S0012-821X(98)00267-2

Li, J., & Agee, C. B. (1996). Geochemistry of mantle-core differentiation at high pressure. *Nature*, *381*(6584), 686–689. https://doi.org/10.1038/381686a0

Lyons, T. W., Reinhard, C. T., & Planavsky, N. J. (2014). The rise of oxygen in Earth's early ocean and atmosphere. *Nature*, *506*(7488), 307–315. https://doi.org/10.1038/nature13068

Marchi, S., Bottke, W. F., Elkins-Tanton, L. T., Bierhaus, M., Wuennemann, K., Morbidelli, A., & Kring, D. A. (2014). Widespread mixing and burial of Earth's Hadean crust by asteroid impacts. *Nature*, *511*(7511), 578–582. https://doi.org/10.1038/nature13539

Marchi, S., Canup, R. M., & Walker, R. J. (2018). Heterogeneous delivery of silicate and metal to the Earth by large planetesimals. *Nature Geoscience*, *11*(1), 77–81. https://doi.org/10.1038/s41561-017-0022-3

Martins, R., Kuthning, S., Coles, B. J., Kreissig, K., & Rehkämper, M. (2023). Nucleosynthetic isotope anomalies of zinc in meteorites constrain the origin of Earth's volatiles. *Science*, *379*(6630), 369–372. https://doi.org/10.1126/science.abn1021

McCollom, T. M. (2013). Miller-urey and beyond: What have we learned about prebiotic organic synthesis reactions in the past 60 years? *Annual Review of Earth and Planetary Sciences*, *41*(1), 207–229. https://doi.org/10.1146/annurev-earth-040610-133457

Miyazaki, Y., & Korenaga, J. (2019a). On the timescale of magma ocean solidification and its chemical consequences: 1. Thermodynamic database for liquid at high pressures. *Journal of Geophysical Research: Solid Earth*, *124*(4), 3382–3398. https://doi.org/10.1029/2018jb016932

Miyazaki, Y., & Korenaga, J. (2019b). On the timescale of magma ocean solidification and its chemical consequences: 2. Compositional differentiation under crystal accumulation and matrix compaction. *Journal of Geophysical Research: Solid Earth*, *124*(4), 3399–3419. https://doi.org/10.1029/2018jb016928

Miyazaki, Y., & Korenaga, J. (2022). A wet heterogeneous mantle creates a habitable world in the Hadean. *Nature*, *603*(7899), 86–90. https://doi.org/10.1038/s41586-021-04371-9

Mondal, P., & Korenaga, J. (2018). The Rayleigh–Taylor instability in a self-gravitating two-layer viscous sphere. *Geophysical Journal International*, *212*(3), 1859–1867. https://doi.org/10.1093/gji/ggx507

Morbidelli, A., & Wood, B. J. (2015). Late accretion and the late veneer. In *The early Earth* (pp. 71–82). https://doi.org/10.1002/9781118860359.ch4

Nakajima, M., Golabek, G. J., Wünnemann, K., Rubie, D. C., Burger, C., Melosh, H. J., et al. (2021). Scaling laws for the geometry of an impact-induced magma ocean. *Earth and Planetary Science Letters*, *568*, 116983. https://doi.org/10.1016/j.epsl.2021.116983

Nakajima, S., Hayashi, Y.-Y., & Abe, Y. (1992). A study on the "runaway greenhouse effect" with a one-dimensional radiative–convective equilibrium model. *Journal of the Atmospheric Sciences*, *49*(23), 2256–2266. https://doi.org/10.1175/1520-0469(1992)049<2256:ASOTGE>2.0.CO;2

Nesvorný, D., Roig, F. V., & Deienno, R. (2021). The role of early giant-planet instability in terrestrial planet formation. *The Astronomical Journal*, *161*(2), 50. https://doi.org/10.3847/1538-3881/abc8ef

Neumann, W., Kruijer, T. S., Breuer, D., & Kleine, T. (2018). Multiestage core formation in planetesimals revealed by numerical modeling and Hf-W chronometry of iron meteorites. *Journal of Geophysical Research: Planets*, *123*(2), 421–444. https://doi.org/10.1002/2017JE005411

Newcombe, M. E., Nielsen, S. G., Peterson, L. D., Wang, J., Alexander, C., Sarafian, A. R., et al. (2023). Degassing of early-formed planetesimals restricted water delivery to Earth. *Nature*, *615*(7954), 854–857. https://doi.org/10.1038/s41586-023-05721-5

Nicklas, R. W., Puchtel, I. S., Ash, R. D., Piccoli, P. M., Hanski, E., Nisbet, E. G., et al. (2019). Secular mantle oxidation across the Archean-Proterozoic boundary: Evidence from V partitioning in komatiites and picrites. *Geochimica et Cosmochimica Acta*, *250*, 49–75. https://doi.org/10.1016/j.gca.2019.01.037

Nimmo, F., O'Brien, D. P., & Kleine, T. (2010). Tungsten isotopic evolution during late-stage accretion: Constraints on Earth–Moon equilibration. *Earth and Planetary Science Letters*, *292*(3–4), 363–370. https://doi.org/10.1016/j.epsl.2010.02.003

O'Brien, D. P., Izidoro, A., Jacobson, S. A., Raymond, S. N., & Rubie, D. C. (2018). The delivery of water during terrestrial planet formation. *Space Science Reviews*, *214*(2018), 47. https://doi.org/10.1007/s11214-018-0475-8

O'Neill, C., & Aulbach, S. (2022). Destabilization of deep oxidized mantle drove the Great Oxidation Event. *Science Advances*, *8*(7), eabg1626. https://doi.org/10.1126/sciadv.abg1626

Poe, B. T., McMillan, P. F., Rubie, D. C., Chakraborty, S., Yarger, J., & Diefenbacher, J. (1997). Silicon and oxygen self-diffusivities in silicate liquids measured to 15 gigapascals and 2800 kelvin. *Science*, *276*(5316), 1245–1248. https://doi.org/10.1126/science.276.5316.1245

Posner, E. S., Rubie, D. C., Frost, D. J., & Steinle-Neumann, G. (2017). Experimental determination of oxygen diffusion in liquid iron at high pressure. *Earth and Planetary Science Letters*, *464*, 116–123. https://doi.org/10.1016/j.epsl.2017.02.020

Qaddah, B., Monteux, J., Clesi, V., Bouhifd, M. A., & Le Bars, M. (2019). Dynamics and stability of an iron drop falling in a magma ocean. *Physics of the Earth and Planetary Interiors*, *289*, 75–89. https://doi.org/10.1016/j.pepi.2019.02.006

Rubie, D. C., Frost, D. J., Mann, U., Asahara, Y., Nimmo, F., Tsuno, K., et al. (2011). Heterogeneous accretion, composition and core–mantle differentiation of the Earth. *Earth and Planetary Science Letters*, *301*(1–2), 31–42. https://doi.org/10.1016/j.epsl.2010.11.030

Rubie, D. C., Melosh, H. J., Reid, J. E., Liebske, C., & Righter, K. (2003). Mechanisms of metal-silicate equilibration in the terrestrial magma ocean. *Earth and Planetary Science Letters*, *205*(3–4), 239–255. https://doi.org/10.1016/S0012-821X(02)01044-0

Rubie, D. C., Nimmo, F., & Melosh, H. J. (2015). Formation of the Earth's core. *Treatise on Geophysics*, 43–79. https://doi.org/10.1016/b978-0-444-53802-4.00154-8

Rudge, J. F., Kleine, T., & Bourdon, B. (2010). Broad bounds on Earth's accretion and core formation constrained by geochemical models. *Nature Geoscience*, *3*(6), 439–443. https://doi.org/10.1038/ngeo872

Salvador, A., & Samuel, H. (2023). Convective outgassing efficiency in planetary magma oceans: Insights from computational fluid dynamics. *Icarus*, *390*, 115265. https://doi.org/10.1016/j.icarus.2022.115265

Schaefer, L., Pahlevan, K., & Elkins-Tanton, L. T. (2024). Ferric iron evolution during crystallization of the Earth and Mars. *Journal of Geophysical Research: Planets*, *129*(9). https://doi.org/10.1029/2023je008262

Sleep, N. H. (2016). Asteroid bombardment and the core of Theia as possible sources for the Earth's late veneer component. *Geochemistry, Geophysics, Geosystems*, *17*(7), 2623–2642. https://doi.org/10.1002/2016gc006305

Solomatov, V. (2015). Magma oceans and primordial mantle differentiation. *Treatise on Geophysics*, *9*, 81–104. https://doi.org/10.1016/b978-0-444-53802-4.00155-x

Sossi, P. A., Burnham, A. D., Badro, J., Lanzirotti, A., Newville, M., & O'Neill, H. S. C. (2020). Redox state of Earth's magma ocean and its Venus-like early atmosphere. *Science Advances*, *6*(48), eabd1387. https://doi.org/10.1126/sciadv.abd1387

Steller, T., Burkhardt, C., Yang, C., & Kleine, T. (2022). Nucleosynthetic zinc isotope anomalies reveal a dual origin of terrestrial volatiles. *Icarus*, *386*, 115171. https://doi.org/10.1016/j.icarus.2022.115171

Stevenson, D. J. (1990). Fluid dynamics of core formation. In *Origin of the Earth* (pp. 231–249). Oxford University Press.

Suer, T. A., Siebert, J., Remusat, L., Day, J. M. D., Borensztajn, S., Doisneau, B., & Fiquet, G. (2021). Reconciling metal-silicate partitioning and late accretion in the Earth. *Nature Communications*, *12*(1), 2913. https://doi.org/10.1038/s41467-021-23137-5

Thiemens, M. M., Sprung, P., Fonseca, R. O. C., Leitzke, F. P., & Münker, C. (2019). Early Moon formation inferred from hafnium–tungsten systematics. *Nature Geoscience*, *12*(9), 696–700. https://doi.org/10.1038/s41561-019-0398-3

Turcotte, D., & Schubert, G. (2014). *Geodynamics* (3rd ed.). Cambridge University Press. https://doi.org/10.1017/CBO9780511843877

Ulvrová, M., Coltice, N., Ricard, Y., Labrosse, S., Dubuffet, F., Velímský, J., & Šrámek, O. (2011). Compositional and thermal equilibration of particles, drops, and diapirs in geophysical flows. *Geochemistry, Geophysics, Geosystems*, *12*(10), Q10014. https://doi.org/10.1029/2011gc003757

Wetherill, G. W. (1990). Formation of the Earth. *Annual Review of Earth and Planetary Sciences*, *18*(1), 205–256. https://doi.org/10.1146/annurev.ea.18.050190.001225

Wood, B. J., Walter, M. J., & Wade, J. (2006). Accretion of the Earth and segregation of its core. *Nature*, *441*(7095), 825–833. https://doi.org/10.1038/nature04763

Zahnle, K. J., Lupu, R., Catling, D. C., & Wogan, N. (2020). Creation and evolution of impact-generated reduced atmospheres of early Earth. *The Planetary Science Journal*, *1*(1), 11. https://doi.org/10.3847/PSJ/ab7e2c

Zahnle, K. J., Lupu, R., Dobrovolskis, A., & Sleep, N. H. (2015). The tethered Moon. *Earth and Planetary Science Letters*, *427*, 74–82. https://doi.org/10.1016/j.epsl.2015.06.058

Zhang, F., Stagno, V., Zhang, L., Chen, C., Liu, H., Li, C., & Sun, W. (2024). The constant oxidation state of Earth's mantle since the Hadean. *Nature Communications*, *15*(1), 6521. https://doi.org/10.1038/s41467-024-50778-z

Zhang, H. L., Hirschmann, M. M., Cottrell, E., & Withers, A. C. (2017). Effect of pressure on $Fe^{3+}/\Sigma Fe$ ratio in a mafic magma and consequences for magma ocean redox gradients. *Geochimica et Cosmochimica Acta*, *204*, 83–103. https://doi.org/10.1016/j.gca.2017.01.023

Zhang, H. L., Hirschmann, M. M., Lord, O. T., Rosenthal, A., Yaroslavtsev, S., Cottrell, E., et al. (2024). Ferric iron stabilization at deep magma ocean conditions. *Science Advances*, *10*(42), eadp1752. https://doi.org/10.1126/sciadv.adp1752

Zube, N. G., Nimmo, F., Fischer, R. A., & Jacobson, S. A. (2019). Constraints on terrestrial planet formation timescales and equilibration processes in the Grand Tack scenario from Hf-W isotopic evolution. *Earth and Planetary Science Letters*, *522*, 210–218. https://doi.org/10.1016/j.epsl.2019.07.001